Synthesis and biological evaluation of novel 2-(benzofuran-2-yl)-chromone derivatives for in vivo imaging of prion deposits in the brain

Mari Nakaie, Fumihiro Katayama, Takehiro Nakagaki, Sakura Yoshida, Masao Kawasaki, Kodai Nishi, Kazuma Ogawa, Akira Toriba, Noriyuki Nishida, Morio Nakayama*, Takeshi Fuchigami*

AUTHOR INFORMATION

Corresponding Authors

Morio Nakayama – Department of Hygienic Chemistry, Graduate School of Biomedical Sciences, Nagasaki University, 1-14 Bunkyo-machi, Nagasaki 852-8521, Japan;

orcid.org/0000-0003-2053-7537; Email: nakmorio@gmail.com*

Takeshi Fuchigami − Laboratory of Clinical Analytical Sciences, Division of Pharmaceutical Sciences, Kanazawa University Graduate School, Kakuma-machi, Kanazawa, Ishikawa 920-1192, Japan;

orcid.org/0000-0001-8141-1212; Email: t-fuchi@p.kanazawa-u.ac.jp*

Authors

Mari Nakaie − Department of Hygienic Chemistry, Graduate School of Biomedical Sciences, Nagasaki University, 1-14 Bunkyo-machi, Nagasaki 852-8521, Japan;

Fumihiro Katayama − Department of Hygienic Chemistry, Graduate School of Biomedical Sciences, Nagasaki University, 1-14 Bunkyo-machi, Nagasaki 852-8521, Japan;

Takehiro Nakagaki − Department of Molecular Microbiology and Immunology, Graduate School of Biomedical Sciences, Nagasaki University, 1-12-4 Sakamoto, Nagasaki 852-8523, Japan;

orcid.org/0000-0003-1960-8326

Sakura Yoshida − Department of Hygienic Chemistry, Graduate School of Biomedical Sciences, Nagasaki University, 1-14 Bunkyo-machi, Nagasaki 852-8521, Japan;

orcid.org/0000-0002-5198-4711

Masao Kawasaki − Department of Hygienic Chemistry, Graduate School of Biomedical Sciences, Nagasaki University, 1-14 Bunkyo-machi, Nagasaki 852-8521, Japan;

Kodai Nishi − Department of Radioisotope Medicine, Atomic Bomb Disease Institute, Nagasaki University, 1-12-4 Sakamoto, Nagasaki 852-8523, Japan;

orcid.org/0000-0002-4919-7639

Kazuma Ogawa − Laboratory of Clinical Analytical Sciences, Graduate School of

Medical Sciences, Kanazawa University, Kakuma-machi, Kanazawa, Ishikawa 920-1192, Japan; Institute for Frontier Science Initiative, Kanazawa University, Kakuma-machi, Kanazawa, Ishikawa 920-1192, Japan;

orcid.org/0000-0002-1691-7302

Akira Toriba − Department of Hygienic Chemistry, Graduate School of Biomedical Sciences, Nagasaki University, 1-14 Bunkyo-machi, Nagasaki 852-8521, Japan;

orcid.org/0000-0002-6411-4088

Noriyuki Nishida − Department of Molecular Microbiology and Immunology, Graduate School of Biomedical Sciences, Nagasaki University, 1-12-4 Sakamoto, Nagasaki 852-8523, Japan;

orcid.org/0000-0001-8737-2488

ABSTRACT

Prion diseases are fatal neurodegenerative disorders caused by deposition of scrapie prion protein aggregates (PrP^{Sc}) in the brain. We previously reported that styrylchromone (SC) and benzofuran (BF) derivatives have potential as imaging probes for PrP^{Sc}. To further improve their properties, we designed and synthesized 2-(benzofuran-2-yl)-chromone (BFC) derivatives hybridized with SC and BF backbones as novel single-photon emission computed tomography probes for the detection of cerebral PrP^{Sc} deposits. Recombinant mouse prion protein (rMoPrP) aggregates and mouse-adapted bovine spongiform encephalopathy (mBSE)-infected mice were used to evaluate the binding properties of BFC derivatives to PrP^{Sc}. The BFC derivatives exhibited high binding affinities (equilibrium dissociation constant [K_d] = 22.6–47.7 nM) for rMoPrP aggregates. All BFC derivatives showed remarkable selectivity against amyloid beta aggregates. Fluorescence microscopy confirmed that the fluorescence signals of the BFC derivatives corresponded to the antibody-positive deposits of PrP^{Sc} in mBSE-infected mouse brains. Among the BFC derivatives, [^{125}I]BFC-OMe and [^{125}I]BFC-NH_2 exhibited high brain uptake and favorable washout from the mouse brain. In vitro autoradiography demonstrated that the distribution of [^{125}I]BFC-OMe in the brain tissues of mBSE-infected mice was co-localized with PrP^{Sc} deposits. Taken together, BFC derivatives

appear to be promising prion imaging probes.

KEYWORDS: Prion disease, PrP^{Sc}, amyloid, 2-(benzofuran-2-yl)-chromone, single photon emission computed tomography (SPECT)

Prion diseases, also known as transmissible spongiform encephalopathies, are incurable, fatal neurodegenerative diseases that affect both humans and animals.[1] Human prion diseases have an annual incidence of 1–2 cases per million people, however, the majority of patients die within a year when clinical symptoms occur.[2, 3] These diseases have been classified as sporadic, genetic, and infectious. Creutzfeldt-Jakob disease (CJD) is the most common prion disease, of which sporadic CJD (sCJD) accounts for 75–85% of the types of CJD.[3, 4] Genetic prion disease is classified as familial CJD, Gerstmann-Sträusler-Scheinker syndrome (GSS), or fatal familial insomnia, depending on specific clinical and pathological features. Kuru, iatrogenic CJD, and variant CJD are infectious diseases that can be caused by external prions.[5] They have a long asymptomatic incubation period; however, severe clinical symptoms develop in a short period of time. Their common pathologies include neuronal loss, spongiform generation, and astrocytic

gliosis in brain tissues.[6] These symptoms are thought to be caused by the misfolding and deposition of scrapie prion protein aggregates (PrP^{Sc}) in the central nervous system (CNS).[7]

No effective treatment for human prion diseases is currently available despite diligent research efforts. At present, an unequivocal diagnosis of prion disease requires neuropathological examination and immunostaining of PrP^{Sc} in the postmortem brain tissue.[8] Therefore, a definitive antemortem diagnosis is urgently required. Since 2010, real-time quaking-induced conversion (RT-QUIC) techniques have emerged as ultrasensitive and specific diagnostic methods for the premortem diagnosis of sCJD.[9, 10] These diagnostic methods are based on the monitoring of thioflavin T (ThT) fluorescence signals which bind to amplified misfolded PrP^{Sc} in biopsy samples (e.g., cerebrospinal fluid and olfactory mucosa) by recombinant PrP. The specificity of RT-QUIC for CJD is markedly high, exceeding 99% for sCJD. Moreover, the sensitivity of this technique is also very high, whereas stable detection sensitivity has not been obtained for infrequent subtypes.[11] Prion diseases are rare, therefore, the development of non-invasive diagnostic techniques other than RT-QUIC is necessary for achieving a more accurate diagnosis of these diseases. Several in vivo imaging techniques have been used to aid in the diagnosis of CJD. Magnetic resonance imaging has achieved sensitive detection of atrophy in prion

diseases and staging of their disease progression.[12] Nuclear medicine imaging, such as single-photon emission computed tomography (SPECT) and positron emission tomography (PET), could perform more disease-specific imaging using appropriate molecular probes.[13] Misfolded PrP^{Sc} has a β-sheet-rich structure that forms amyloid fibrils such as beta-amyloid (Aβ) plaques, which are characteristic of Alzheimer's disease.[14] Accordingly, several PET imaging probes that originally targeted Aβ have been evaluated to visualize PrP^{Sc} in the brain tissue of patients with prion disease. However, inconsistent results, including some samples and negative reports, have impeded their usefulness in clinical practice. Therefore, these probes have not been verified as diagnostic tools.[15] In contrast, [^{18}F]FDDNP (Figure 1) localization in several brain regions of PRNP F198S GSS patients,[16] [^{11}C]PIB and [^{11}C]BF-227, (Figure 1) failed to detect deposits in patients with GSS and CJD, respectively.[17] We previously developed a series of radioligands, including flavonoids,[18, 19, 20, 21] acridines,[22, 23] and benzofurans,[24, 25] as new imaging probes for PrP^{Sc} and Aβ (Fig. 1). Among them, [^{123}I]SC-OMe (Figure 1), a styrylchromone derivative, allowed to visualize prion deposits in mouse-adapted bovine spongiform encephalopathy (mBSE)-infected mice, a typical model of prion disease,[26] using a small animal SPECT/CT imaging system.[20] However, inadequate blood-brain barrier (BBB) permeability can hinder the clinical application of [^{123}I]SC-OMe. Another disadvantage

of SC derivatives is that photoisomerization may prevent the reproducibility of PrP^{Sc} imaging. More recently, we reported that [^{123}I]IPBF-NHMe (Figure 1) successfully visualized prion deposits in living brain tissues of mBSE-infected mice by SPECT.[27] However, this radiotracer also exhibited high affinity for $A\beta_{1–42}$ aggregates,[28] which could be an obstacle for the clinical imaging of PrP^{Sc}. Therefore, continued efforts are required to develop new imaging probes with improved brain distribution and binding selectivity for PrP^{Sc}, which could allow for PrP^{Sc}-specific in vivo imaging. We hypothesized that novel derivatives combining the backbone of SC and BF could be used as prospective prion imaging probes. In this study, we developed 2-(benzofuran-2-yl)-chromone (BFC) derivatives hybridized with SC and BF as novel PrP^{Sc} imaging probes (Figure 2). Unlike SC, photoisomerization cannot occur in BFCs; thus, each BFC derivative is expected to provide reproducible imaging with a single compound. We designed four radioiodinated BFC derivatives with electron-donating groups (-OMe, $-NH_2$, -NHMe, and $-NMe_2$), which play important roles in the binding affinity to amyloid,[29] for PrP^{Sc} imaging. Recently, a CNS multiparameter optimization (CNS MPO) and a CNS PET multiparameter optimization (CNS PET MPO) algorithm was developed to predict the preferred physicochemical properties of clinically useful CNS PET tracers.[30, 31] This algorithm includes calculated logP (ClogP), calculated distribution coefficient at pH = 7.4

(ClogD), molecular weight (MW), topological polar surface area (TPSA), number of hydrogen bond donors (HBD), and ionization constant of the most basic center (pK_a). While the preferred range of CNS MPO was set as ClogP ≤ 3.0, ClogD ≤ 2.0, MW ≤ 360, 40 < TPSA ≤ 90, HBD ≤ 0.5, and pK_a ≤ 8.0,[30] the preferred range of CNS PET MPO was set as ClogP ≤ 2.8, ClogD ≤ 1.7, MW ≤ 305.3, 44.8 < TPSA ≤ 63.3, HBD ≤ 1, and pK_a ≤ 7.2.[31] The score range for each parameter was 0–1. The inflection points and desired ranges for the CNS PET MPO tool were derived from the physicochemical property data of commercially available CNS drugs in the CNS MPO article. These values are considered valid for predicting more narrowly defined drugs such as those associated with CNS PET ligands.[31] It has been reported that the majority of marketed CNS drugs have CNS MPO scores > 4 and valid CNS PET tracers have CNS PET MPO scores > 3.[30, 31] Fortunately, the CNS MPO and CNS PET MPO calculation values indicated that the BFC derivative with four electron-donating groups showed higher scores (3.6–4.5 and 2.9–4.0, respectively) than SC-OMe (3.0 and 1.3, respectively) and 5-IBF-NHMe, an *N*-methylamino-substituted BF derivative (3.3 and 2.0, respectively) (Table 1). Therefore, these BFC derivatives was expected to possess high binding affinity for PrP^{Sc} and high BBB permeability. Herein, we describe the synthesis and evaluation of BFC derivatives as prion-imaging probes. Although ^{123}I ($t_{1/2}$ = 13.3 hours) has been used for SPECT probes,

^{125}I ($t_{1/2}$ = 59.4 days), which has a long half-life and is easy to handle, was used in this fundamental research.

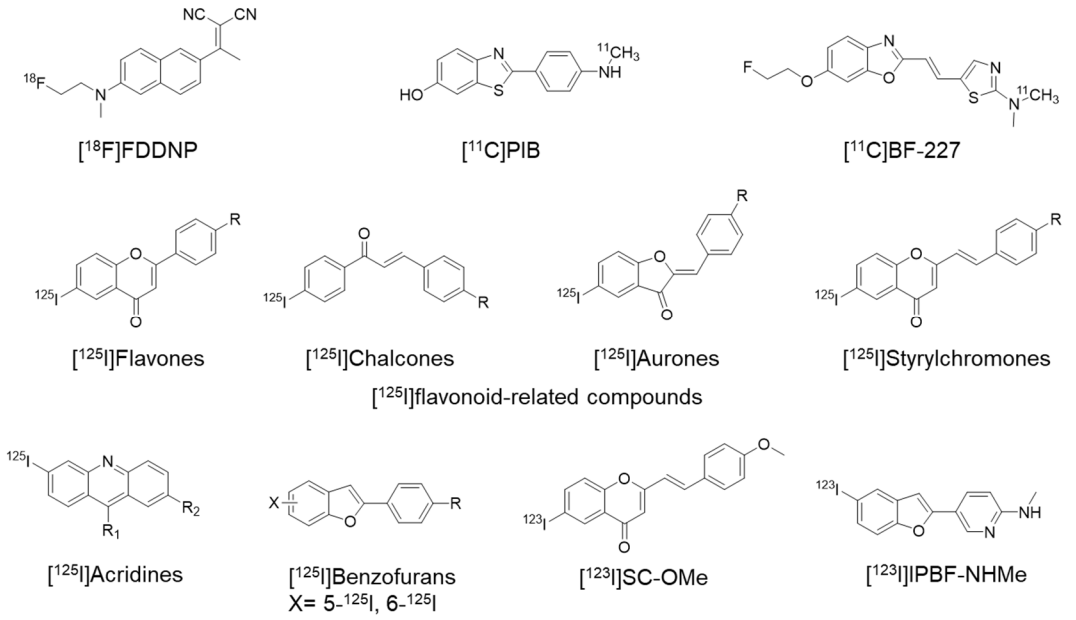

Figure 1. Chemical structures of reported imaging probes for scrapie prion protein (PrP^{Sc}).

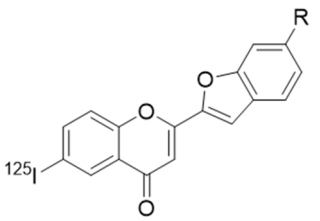

Figure 2. Chemical structures of 2-(benzofuran-2-yl)-chromone (BFC) derivatives evaluated as scrapie prion protein (PrP^{Sc}) imaging probes in this study.

Table 1. Individual CNS PET MPO parameters of SC-OMe, 5-IBF-NHMe, and BFC derivatives

Compound	ClogP[a]	ClogD[b]	TPSA[a]	MW	HBD	pK_a[b]	CNS MPO[c]	CNS PET MPO[c]
SC-OMe	4.14	6.00	35.53	404.20	0	9.70	3.0	1.3
5-IBF-NHMe	4.23	5.02	21.26	349.17	1	3.88	3.3	2.0
IPBF-NHMe	3.61	4.93	33.62	350.16	1	4.61	4.2	2.4
BFC-OMe	2.95	5.76	44.76	418.19	0	10.41	3.6	2.9
BFC-NH_2	2.27	4.68	61.55	403.18	1	3.31	4.5	4.0
BFC-NHMe	2.57	5.17	47.56	417.20	1	3.68	4.4	4.0
BFC-NMe_2	3.36	5.57	38.77	431.23	0	3.91	4.2	3.1

[a] The physicochemical properties of each compound was calculated using a ChemBioDraw Ultra 20.1.

[b] The physicochemical properties of each compound was calculated using a SPARK on line calculator.

[c] The CNS PET MPO of each compound was calculated according to the literature.[30, 31]

ClogP, calculated partition coefficient; ClogD, calculated distribution coefficient at pH=7.4; MW, molecular weight; TPSA, topological polar surface area; HBD, number of hydrogen bond donors, pK_a, ionization constant of the most basic center.

RESULTS AND DISCUSSION

Chemistry. The synthetic route to the target BFC derivatives is shown in Scheme 1. The 2-methoxy-4-nitrobenzaldehyde was desmethylated with boron tribromide (BBr_3) to provide **1** at a 79% yield. 2-Hydroxy-4-methoxybenzaldehyde and **1** were allowed to react with ethyl bromoacetate to form benzofurans **2** and **3** in 15% and 16% yields, respectively. The hydrolysis of **2** and **3** with NaOH produced **4** and **5** in 69% and 45% yields, respectively. Compounds **6** and **7** were formed by the esterification of **4** or **5** and 5'-bromo-2'-hydroxyacetophenon (71% and 99% yields, respectively). The 1,3-diketones **8** and **9** were formed by the rearrangement of **6** and **7** with KOH (17% and 41% yields, respectively). The cyclodehydration of **8** and **9** by refluxing with sulfuric and acetic acids yielded 72% and 51% of 6-bromo derivatives **10** and **11**, respectively. The amino derivative **13** was prepared from **11** by reduction with $SnCl_2$ (89% yield). Conversion of **13** to monomethylamino derivative **15** was performed using paraformaldehyde, sodium

methoxide (NaOMe), and sodium tetrahydridoborate ($NaBH_4$) at a 22% yield. Compound **11** was converted to dimethylamino derivative **17** using paraformaldehyde, sodium cyanoborohydride ($NaCNBH_3$), and acetic acid (71% yield). Treatment of **10**, **13**, **15**, and **17** with tributyltin hydride [$(SnBu_3)_2$] and tetrakis(triphenylphosphine)palladium(0) [$(PPh_3)_4Pd$] generated the tributyltin derivatives **12**, **14**, **16**, and **18** (15%, 9%, 41%, 27% yield, respectively). The targets BFC-OMe, BFC-NH_2, BFC-NHMe, and BFC-NMe_2 were synthesized using a tributyltin-to-iodine exchange reaction from the corresponding tributyltin derivatives at yields of 88%, 88%, 87%, and 92%, respectively. Radioiodination of the BFC derivatives was achieved using an iododestannylation reaction with hydrogen peroxide as an oxidant, which produced the desired radioiodinated ligands at 15–96% yields (Scheme 2).

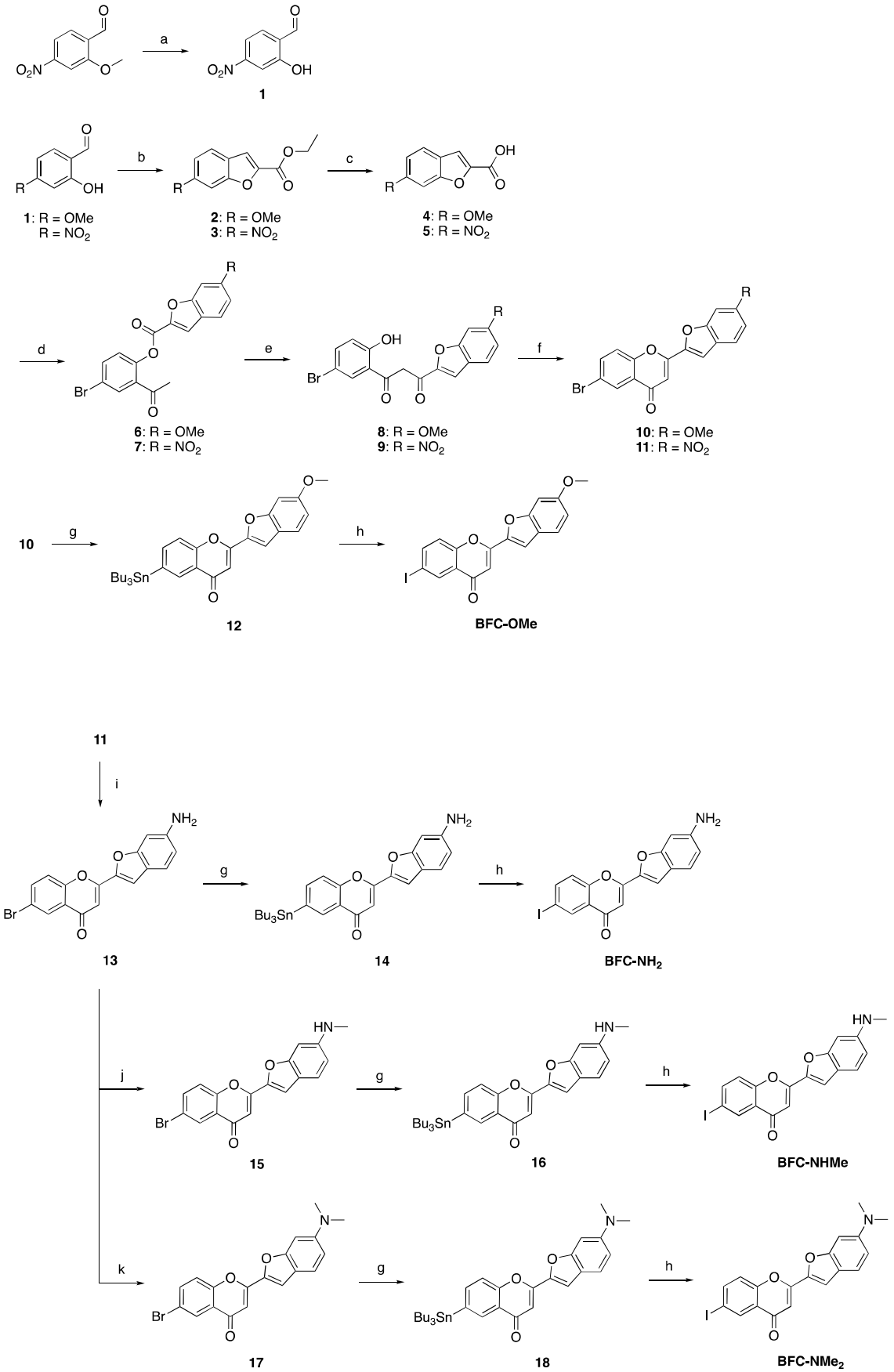
a
1
b
c
1: R = OMe
R = NO2
2: R = OMe
3: R = NO2
4: R = OMe
5: R = NO2
d
e
f
6: R = OMe
7: R = NO2
8: R = OMe
9: R = NO2
10: R = OMe
11: R = NO2
10
g
h
12
BFC-OMe
11
i
g
h
13
14
BFC-NH2
j
g
h
15
16
BFC-NHMe
k
g
h
17
18
BFC-NMe2

Scheme 1. Synthesis of benzofuranyl chromone (BFC) derivatives.

Reagents and conditions: (a) BBr_3, CH_2Cl_2, rt, 4 h; (b) Ethyl bromoacetate, K_2CO_3, DMF, 80-90 °C, 6-18 h; (c) NaOH, MeOH, rt, 2 h; (d) 5'-bromo-2'-hydroxyacetophenone, phosphoryl chloride, pyridine, rt, 2-12 h; (e) KOH, pyridine, rt, 2 h; (f) H_2SO_4, AcOH, 100 °C, 2 h; (g) $(SnBu_3)_2$, Pd $(PPh_3)_4$, dioxane, TEA, 80-90 °C, 14 h; (h) I_2, $CHCl_3$, rt, 2-3 h; (i) $SnCl_2$, EtOH, 100 °C, 3 h; (j) CH_3ONa, $(CH_2O)_n$, MeOH, reflux, 1 h; $NaBH_4$, reflux, 3 h; (k) $NaCNBH_3$, $(CH_2O)_n$, AcOH, rt, 4 h.

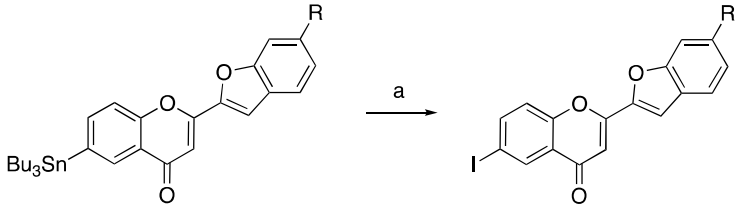

12: R = OMe
14: R = NH_2
16: R = NHMe
18: R = NMe_2

[^{125}I]BFC-OMe: R = OMe
[^{125}I]BFC-NH_2: R = NH_2
[^{125}I]BFC-NHMe: R = NHMe
[^{125}I]BFC-NMe2: R = NMe_2

Scheme 2. Radiosynthesis of ^{125}I-labeled BFC derivatives.

Reagents and conditions: (a) [^{125}I]NaI, H_2O_2, HCl, EtOH, rt, 10-20 min.

HPLC analysis of BFC derivatives. Reversed-phase HPLC analysis confirmed that cyclizing the BFC derivatives with styryl groups did not cause photoisomerization

(Figure 3). The SC derivative [^{125}I]SC-NMe$_2$ showed two peaks owing to photoisomerization (Figure 3A). In contrast, only a single major peak of the ^{125}I-labeled BFC derivatives was observed (Figures 3B–E). These results indicate that none of the BFC derivatives underwent photoisomerization.

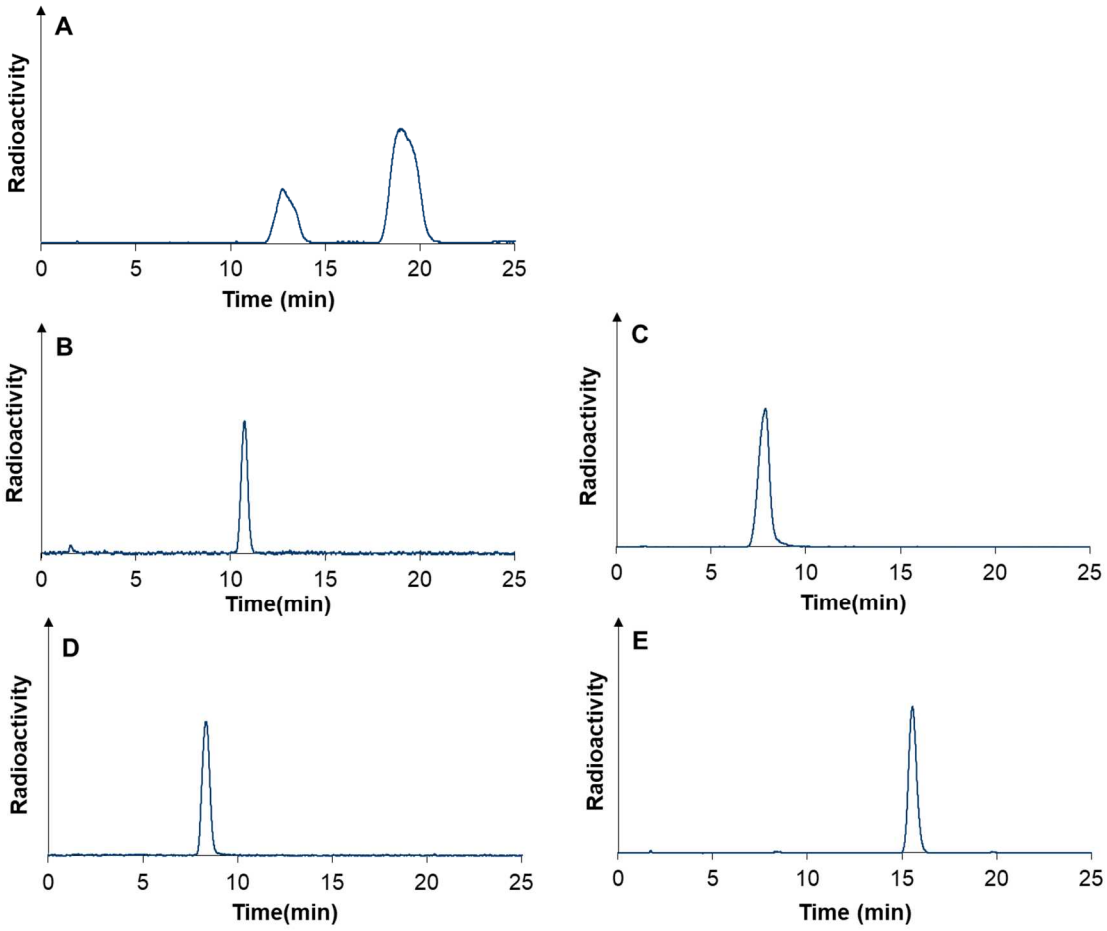

Figure 3. HPLC chromatograms of ^{125}I-labeled SC derivative (SC-NMe_2) (A) and BFC derivatives [BFC-OMe (B), BFC-NH_2 (C), BFC-NHMe (D), and BFC-NMe_2 (E)]. HPLC conditions: Column; Cosmosil 5C_{18}-AR-II (4.6 × 150 mm). Flow rate; 1.0 mL/min. Mobile phase; CH_3CN/H_2O (7/3) [(A), (B), (D), and (E)] and CH_3CN/H_2O (6/4) (C).

In vitro binding of BFC derivatives to amyloids. We previously conducted in vitro screening of candidate prion imaging probes using rMoPrP aggregates as a PrP^{Sc} model.[20, 24, 27] First, an in vitro saturation binding assay of BFC derivatives was performed using the PrP^{Sc} model (Figure 4). The binding of ^{125}I-labeled BFC derivatives to rMoPrP aggregates exhibited a saturated binding curve and a linear Scatchard plot that fitted the single-binding site model (Figure 4). ^{125}I-labeled BFC derivatives had an equilibrium dissociation constant (K_d) and binding capacity (B_{max}) in the ranges of 22.6 to 47.7 nM and 12.6 to 29.3 mmol/mol protein, respectively (Table. 2). In our previous study, [^{125}I]SC-NMe_2, a dimethylamino-substituted SC derivative, and [^{125}I]5-IBF-NHMe had K_d values of 24.5 nM[20] and 12.3 nM,[24] respectively. Therefore, it is suggested that BFC derivatives have high binding affinities equivalent to those of SC and BF derivatives. The BFC derivatives with an amino group at the 4'-position showed binding affinities of

[^{125}I]BFC-NMe$_2$ > [^{125}I]BFC-NHMe > [^{125}I]BFC-NH$_2$, suggesting that the introduction of hydrophobic electron-donating groups at the 4'-position of BFC derivatives improves the binding affinities to rMoPrP aggregates. To elucidate the selectivity of the BFC derivatives for amyloids, their binding affinities to A$\beta_{1\text{-}42}$ aggregates were also evaluated (Table 2). The K_d values of the BFC derivatives for the A$\beta_{1\text{-}42}$ aggregates ranged from 109–259 nM. In contrast, the K_d value of [^{125}I]SC-NMe$_2$ for the A$\beta_{1\text{-}42}$ aggregates was 19.7 ± 3.89 nM. Therefore, it is suggested that the BFC derivatives have much higher binding selectivity for rMoPrP aggregates than those of the SC derivatives. The reason for this deviation in binding affinity is unknown, however, one possible explanation is that the amino acid sequence and shape of each amyloid differ.

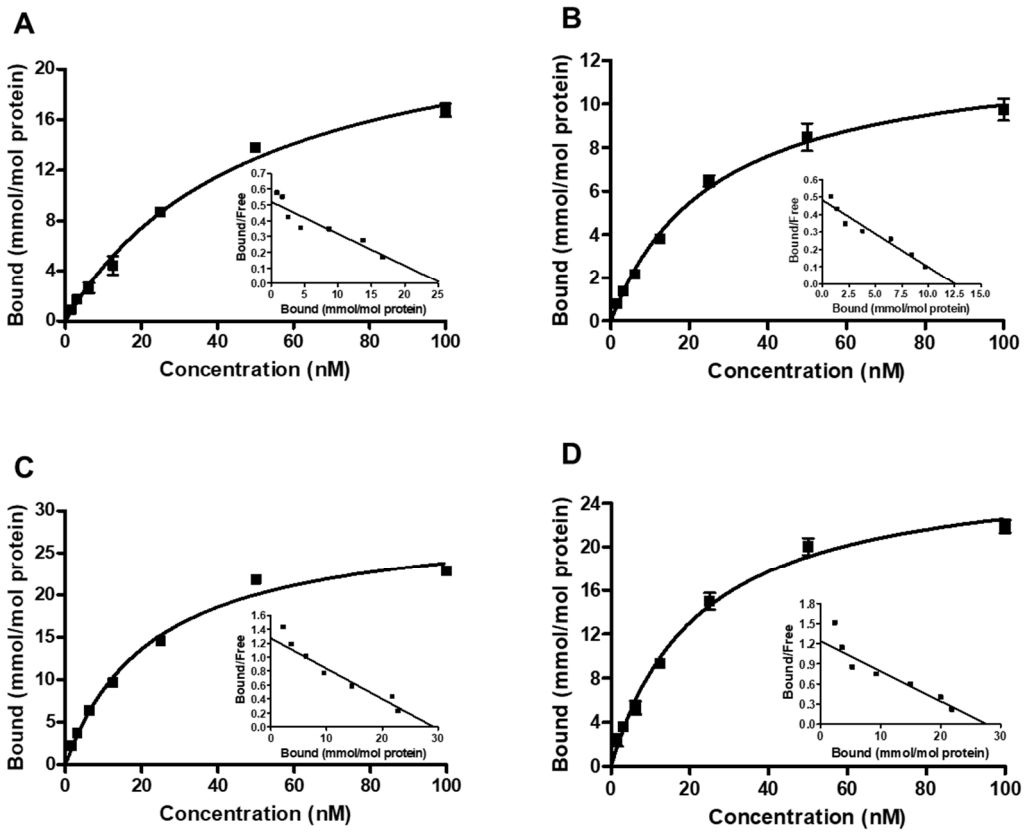

Figure 4. Saturation curve and Scatchard plot of ^{125}I-labeled BFC derivatives bound to rMoPrP aggregates. K_d and B_{max} values were determined via saturation assays using increasing concentrations of [^{125}I]BFC-OMe (A), [^{125}I]BFC-NH_2 (B), [^{125}I]BFC-NHMe (C), [^{125}I]BFC-NMe_2 (D) (1.6-100 nM). Values are the mean ± SEM of three to four independent measurements.

Table 2. The equilibrium dissociation constant (K_d) values of ^{125}I-labeled BFC derivatives to rMoPrP and A$\beta_{1\text{-}42}$ aggregates.

Compounds	K_d (nM)[a]		B_{max} (mmol/mol protein)[a]	
	rMoPrP	A$\beta_{1\text{-}42}$	rMoPrP	A$\beta_{1\text{-}42}$
BFC-OMe	47.7 (2.81)	143 (4.65)	25.6 (0.24)	315 (20.3)
BFC-NH_2	26.1 (2.06)	109 (24.5)	12.6 (0.91)	93.2 (25.8)
BFC-NHMe	23.1 (1.05)	251 (31.9)	29.3 (0.61)	249 (14.8)
BFC-NMe_2	22.6 (1.97)	259 (20.7)	27.6 (0.23)	440 (57.4)
SC-NMe_2	24.5[b]	19.7 (3.89)	36.3[b]	66.8 (4.15)

[a] Values are the mean (SEM) for three to four independent measurements.

[b] Data from previous report.[20]

Fluorescence staining of BFC derivatives in mBSE-infected and *Tg2576* mouse brain sections. BFC derivatives have high binding affinities for rMoPrP aggregates, therefore, the neuropathological fluorescence staining of BFC-OMe, BFC-NH_2, BFC-

NHMe, and BFC-NMe_2 in brain sections from mBSE- and mock-infected mice was further evaluated (Figure 5). The brain sections of mBSE- and mock-infected mice were prepared according to previously reported methods.[20, 23] In the brain sections of mock-infected mice, fluorescent images stained with BFC derivatives were not clearly observed (Figures 5A–D). Conversely, BFC derivatives showed clear fluorescence signals in the brain sections of mBSE-infected mice (Figures 5E–H) and the fluorescent images corresponded to PrP^{Sc} deposits confirmed by the anti-PrP antibody (Figures 5I–L). Therefore, it was suggested that BFC derivatives could recognize PrP^{Sc} deposits in mBSE-infected mouse brain sections. To investigate the binding of BFC derivatives to other amyloid deposits in the brain, fluorescence staining was performed on brain sections from *Tg2576* mice that overexpress amyloid precursor protein and form Aβ plaques[32] (Figure 6). Almost no significant fluorescence signals of BFC-OMe were observed in the brain slices of *Tg2576* mice (Figure 6A) with ThT-positive Aβ plaque regions (Figure 6E). Other BFC derivatives were observed (Figures 6B–D) in parts of the Aβ plaque regions (Figures 6F–H), however, the fluorescence signals were weak. There are several discrepancies between K_d values for $A\beta_{1–42}$ aggregates and the intensity of fluorescence signals in *Tg2576* mice of BFC derivatives. For example, BFC-OMe, which had the second-highest affinity for $A\beta_{1–42}$ aggregates among the BFC derivatives, had the lowest

fluorescence signals in the brain sections of *Tg2576* mice. It has been reported that amyloid plaques in the brain tissues of *Tg2576* mice contain various endogenous substances such as superoxide dismutases and lipid membranes damaged by reactive oxygen species.[33] Therefore, the reason for the differences in the binding properties of BFC derivatives to $A\beta_{1-42}$ aggregates and brain sections from *Tg2576* mice might be because $A\beta_{1-42}$ peptide aggregates and Aβ plaques from *Tg2576* mice share a common $A\beta_{1-42}$ aggregates core, but have different compositions. Nevertheless, these results suggest that BFC derivatives have only a weak binding affinity for Aβ plaques in the brain tissue of *Tg2576* mice, unlike prion deposits in the brain tissue of mBSE-infected mice.

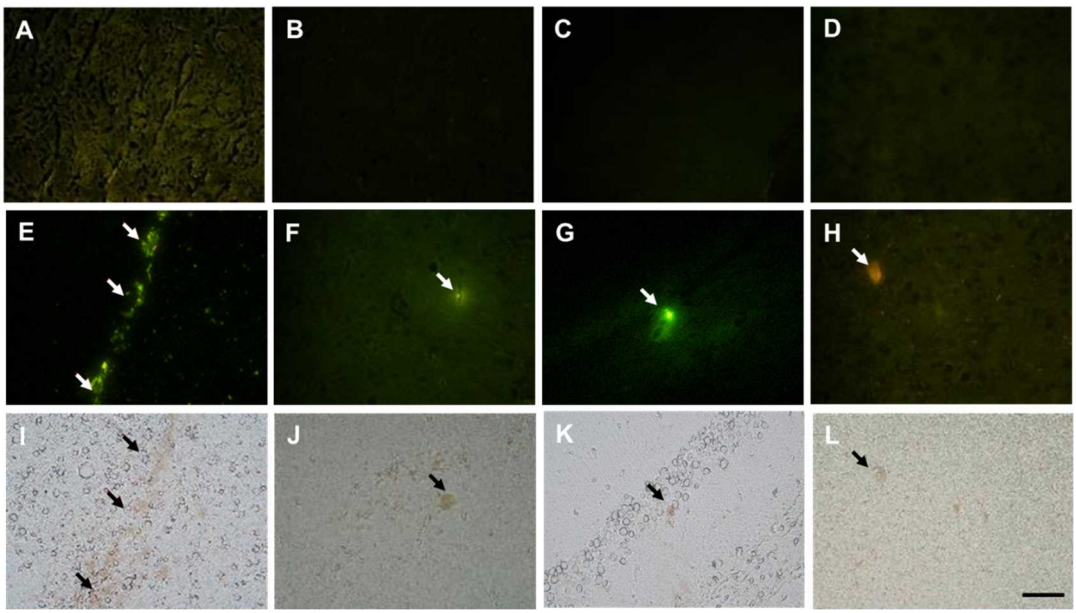

Figure 5. Fluorescence staining of BFC derivatives (BFC-OMe, BFC-NH_2, BFC-NHMe, and BFC-NMe_2) in brain sections of mock-infected (A-D) and mouse-adapted bovine spongiform encephalopathy (mBSE)-infected mice (E–H). Scrapie prion protein (PrP^{Sc}) plaques were confirmed using anti-PrP antibody (I-L). Scale bar = 50 μm.

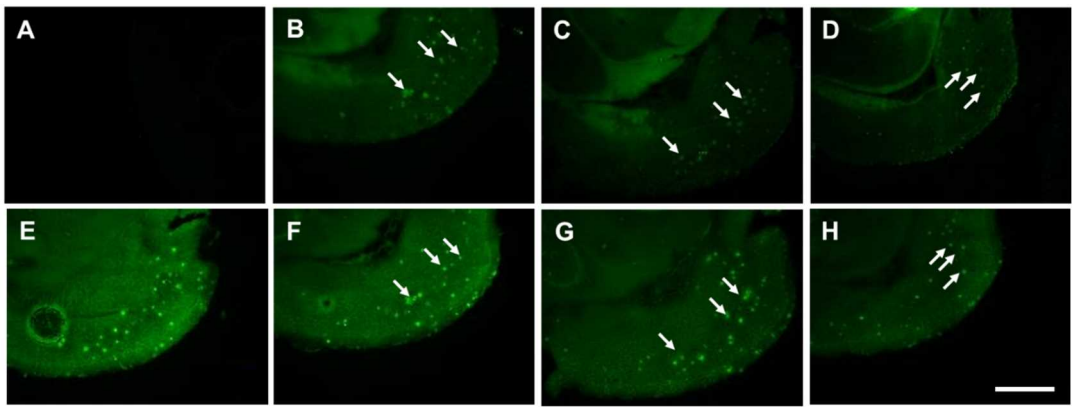

Figure 6. Fluorescence staining of BFC derivatives (BFC-OMe, BFC-NH_2, BFC-NHMe, and BFC-NMe_2) in brain sections of *Tg2576* mice (A-D). The Aβ plaques in brain sections of *Tg2576* mice were confirmed by thioflavin T (E-H). Scale bar = 1.0 mm.

In vivo biodistribution in normal mice. Clinically available in vivo imaging probes for PrP^{Sc} should exhibit good brain penetration and low nonspecific binding to the off-target brain regions. Biodistribution studies of ^{125}I-labeled BFC derivatives in normal mice were performed to evaluate whether BFC derivatives could function as useful in vivo imaging probes. The brain distribution and peripheral region data were expressed as the percentage of injected dose (% ID) or %ID per gram (% ID/g) as shown in Figures 7-9 and Table S1. All ^{125}I-labeled BFC derivatives reached their maximum blood radioactivity levels after 2 min, of which [^{125}I]BFC-NHMe showed the highest value (10% ID/g). Brain uptake in the early phase (2 and 30 min after injection in mice) of ^{125}I-labeled BFC derivatives [^{125}I]BFC-OMe, [^{125}I]BFC-NH_2, [^{125}I]BFC-NHMe, and [^{125}I]BFC-NMe_2 was shown to be up to 4.22, 5.06, 3.08, and 3.16% ID/g, respectively (Figure 7). Therefore, their initial uptake in the brain was higher than that of [^{125}I]SC-OMe (2.25% ID/g at 2 min), which is the most brain-generatable SC derivative.[18] Although the [^{125}I]IPBF-NHMe derivative had high BBB permeability [4.17% injected dose (ID)/g at 2 min post-injection],[27] it is worth noting that [^{125}I]BFC-Me and [^{125}I]BFC-NH_2 had better initial uptake than [^{125}I]IPBF-NHMe. [^{125}I]BFC-OMe exhibited an excessive decrease in brain uptake, even at 10 min, compared to 2 min. The brain uptake of [^{125}I]BFC-OMe, [^{125}I]BFC-NH_2, [^{125}I]BFC-NHMe, and [^{125}I]BFC-NMe_2 in the late

phase 180 min after injection was 0.26%, 0.34%, 1.13%, and 0.28% ID/g, respectively (Figure 7). Therefore, these BFC derivatives, except for BFC-NHMe, demonstrated preferable brain washout. In particular, [^{125}I]BFC-OMe and [^{125}I]BFC-NH_2 had excellent initial BBB permeability and good disappearance from the normal brain tissue. The initial brain uptake was consistent with the CNS MPO and PET MPO scores (Tables 1 and S1). The BFC derivatives and [^{125}I]IPBF-NHMe with high physicochemical scores showed higher initial brain uptake than [^{125}I]SC-OMewith lower scores.[18, 28] However, [^{125}I]BFC-OMe, with the lowest CNS MPO and CNS PET MPO among the BFC derivatives, showed good initial brain penetration and rapid clearance from the normal brain, suggesting that other factors are involved in brain pharmacokinetics. The brain uptake ratio at 2 min ($brain_{2\ min}$)/ 60 min ($brain_{60\ min}$) in normal mice is frequently used as an index parameter for comparing the washout rates of amyloid imaging probes.[34, 35] The $brain_{2\ min}$/$brain_{60\ min}$ ratios of [^{18}F]Florbetapir and [^{18}F]Florbetaben used clinically as PET imaging agents for Aβ aggregates were 3.8[36] and 4.8[34], respectively. In contrast, the $brain_{2\ min}$/$brain_{60\ min}$ ratios of [^{125}I]BFC-OMe and [^{125}I]BFC-NH_2 were 5.8 and 2.6, respectively. Accordingly, [^{125}I]BFC-OMe has a more favorable index parameter than those of clinically used imaging probes. The $brain_{2\ min}$/$brain_{120\ min}$ and $brain_{2\ min}$/$brain_{180\ min}$ ratios of [^{125}I]BFC-NH_2 were 5.7 and 14.9, respectively, indicating that this radioligand

exhibited good washout properties from normal brain tissue. Comparison of ^{125}I-labeled BFC derivatives with amino groups ([^{125}I]BFC-NH_2, [^{125}I]BFC-NHMe, and [^{125}I]BFC-NMe_2) showed that compounds with lower hydrophilicity tended to have better brain uptake and washout in mice. These ^{125}I-labeled BFC derivatives exhibited an overall high initial hepatic uptake. The intestinal uptake gradually increased, indicating that these radioligands were primarily eliminated via biliary excretion (Figure 8). Several abnormal biodistribution patterns of ^{125}I-labeled BFC derivatives were observed, such as spleen uptake of [^{125}I]BFC-NH_2 at 60 min and liver and spleen uptake of [^{125}I]BFC-NH_2 at 60 min. The reasons for these BFC derivatives exhibiting such a biodistribution pattern are unclear. However, the excretion process might have caused hyperaccumulation in certain organs owing to recirculation or other factors. Free radioactive iodine ions produced by deiodination are known to accumulate in the stomach and thyroid gland.[37] Therefore, we chose the uptake in these organs as an indicator of deiodination. The accumulation of [^{125}I]BFC-OMe, [^{125}I]BFC-NH_2, [^{125}I]BFC-NHMe, and [^{125}I]BFC-NMe_2 in the stomach at 180 min was 5.04, 1.41, 1.76, and 0.51% ID, respectively. [^{125}I]BFC-OMe, [^{125}I]BFC-NH_2, [^{125}I]BFC-NHMe, and [^{125}I]BFC-NMe_2 exhibited 0.80, 0.01, 0.08, and 0.04% ID of uptake in the thyroid gland at 180 min, respectively (Figure 9). There results suggested that [^{125}I]BFC-OMe and [^{125}I]BFC-NHMe are more likely to produce free radioiodine

ions than other derivatives are. However, all BFC derivatives showed a gradual decrease in brain uptake over time, suggesting that the re-influx of metabolites into brain tissue is unlikely to occur.

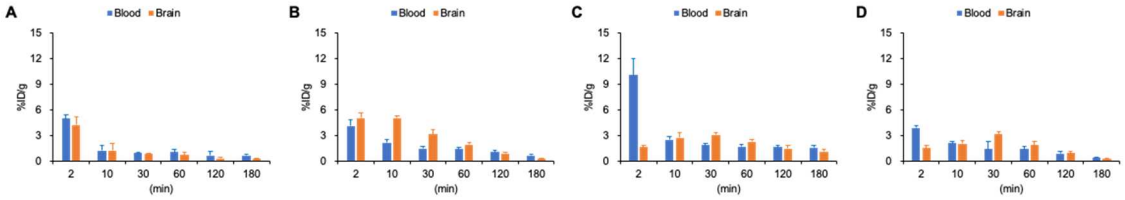

Figure 7. Blood and brain distribution of the radioactivity after intravenous administration of [^{125}I]BFC-OMe (A), [^{125}I]BFC-NH_2 (B), [^{125}I]BFC-NHMe (C), and [^{125}I]BFC-NMe_2 (D) in mice. Data are expressed as percent injected dose per gram (%ID/g). Each value represents the mean ± standard deviation (SD) of 4−6 mice.

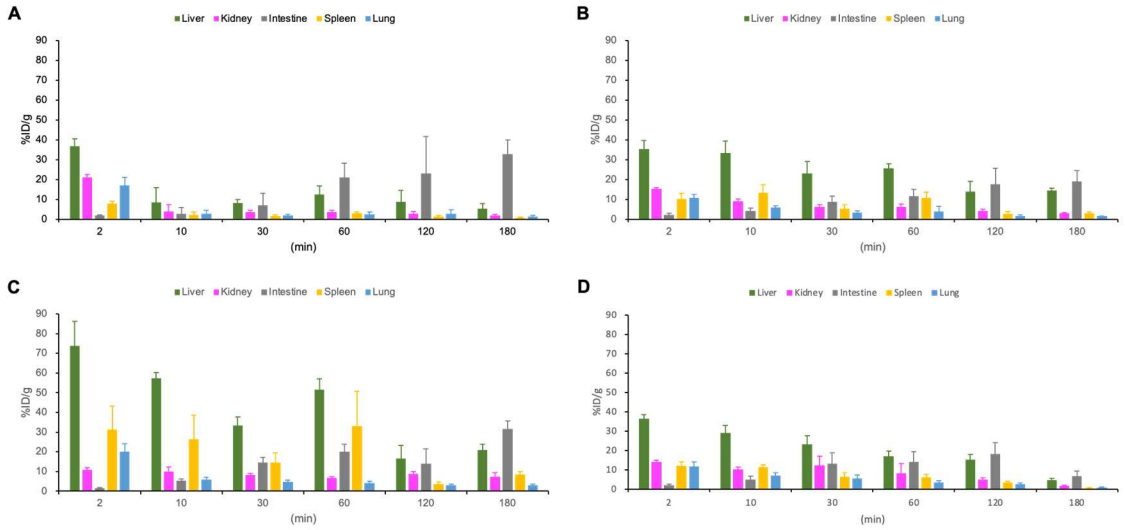

Figure 8. Biodistribution of the radioactivity after intravenous administration of

[^{125}I]BFC-OMe (A), [^{125}I]BFC-NH_2 (B), [^{125}I]BFC-NHMe (C), and [^{125}I]BFC-NMe_2 (D) in the peripheral organs of mice. Data are expressed as %ID/g. Each value represents the mean ± SD of 4−6 mice.

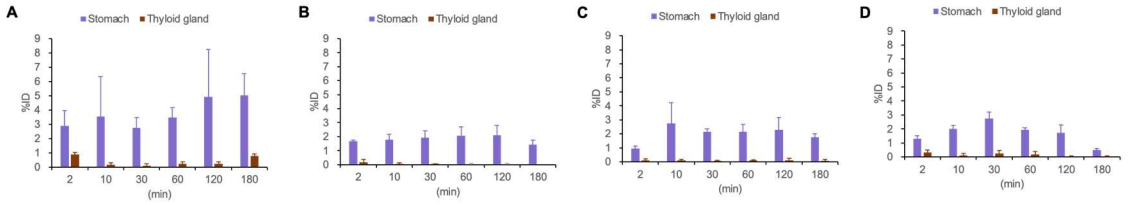

Figure 9. Stomach and thyroid gland distribution of the radioactivity after intravenous administration of [^{125}I]BFC-OMe (A), [^{125}I]BFC-NH_2 (B), [^{125}I]BFC-NHMe (C), and [^{125}I]BFC-NMe_2 (D) in mice. Data are expressed as percent injected dose (%ID). Each value represents the mean ± SD of 4−6 mice.

In vitro autoradiography of [^{125}I]BFC-OMe in mBSE- and mock-infected mouse brain sections. Finally, in vitro autoradiography (ARG) studies were performed in mBSE- and mock-infected mouse brain sections using [^{125}I]BFC-OMe, which is the most favorable in vivo brain distribution among the BFC derivatives. [^{125}I]BFC-OMe exhibited high signals in mBSE-infected mouse brain sections (Figure 10A), which matched the

distribution of PrP^{Sc} deposits (Figures 10C and E). In mock-infected mouse brain sections, [^{125}I]BFC-OMe signals showed a uniform distribution (Figure 10B), and PrP^{Sc} deposits were not shown to be significant (Figures 10D and F). We also conducted in vitro ARG of brain sections from *Tg2576* mice and age-matched control mice, which showed no apparent colocalization of [^{125}I]BFC-OMe and Aβ plaques (Figure S1).

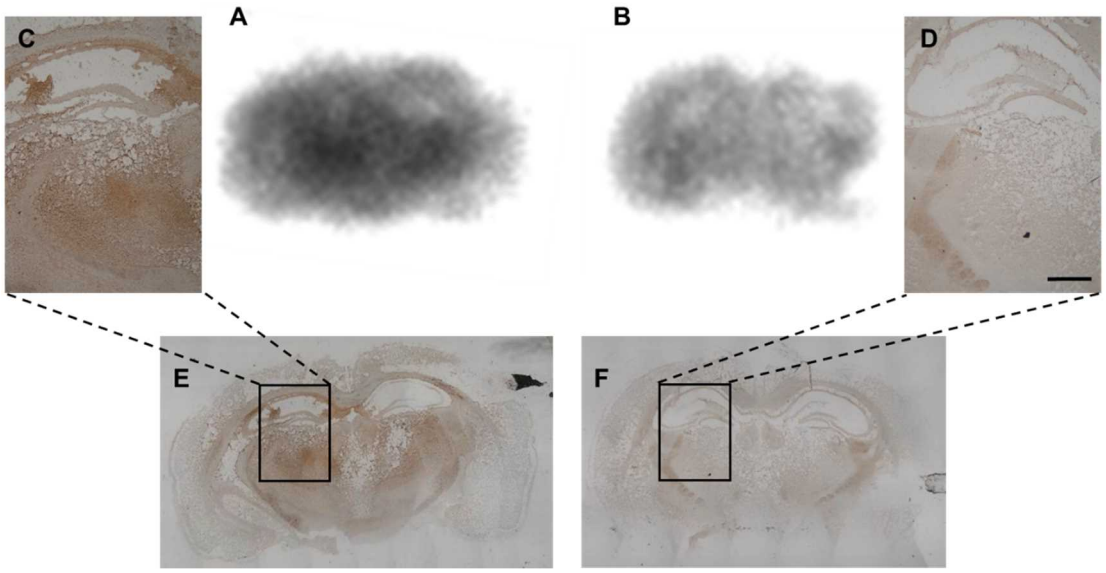

Figure 10. In vitro autoradiograms of the mBSE-infected (A) and mock-infected (B) mice brain labeled with [^{125}I]BFC-OMe. The PrP^{Sc} plaques were confirmed in the mBSE- (C, E) and mock-infected (D, F) mice using anti-PrP antibody. Scale bar = 500 μm.

Taken together, [^{125}I]BFC-OMe has a high binding affinity for PrP^{Sc} and exhibits desirable brain distribution, making it a potentially valuable in vivo imaging probe for PrP^{Sc}. Considering the correlation between binding affinity and chemical backbones of SC, BF, and BFC derivatives, BF derivatives tend to exhibit a higher binding affinity for PrP^{Sc} than did other derivatives, but only BFC derivatives have amyloid binding selectivity for PrP^{Sc} against Aβ. Most of methylamino and dimethylamino derivatives exhibited superior binding affinity for rMoPrP aggregates than did methoxy and amino derivatives.[20, 24, 27] In contrast, methoxy derivatives exhibited superior initial brain uptake and rapid brain wash-out compared to other related analogs of SC[20] and BFC derivatives. The methoxy derivatives exhibit a high affinity for PrP^{Sc} and good brain distribution, but the affinity may need further improvement to serve as effective *in vivo* imaging agents. To the best of our knowledge, there are no reports regarding to determine the exact concentration of PrP^{Sc} using antibodies against PrP and B_{max} of amyloid imaging agents using brain homogenates in clinical specimens from patients with prion diseases. Detailed binding properties of prion imaging probes including BFC derivatives for human brain homogenates from prion disease patients should be examined to speculate the required binding properties of prion imaging probes in the future studies. The major advantages of [^{125}I]BFC-OMe are its binding specificity for PrP^{Sc} compared to $Aβ_{1–42}$ and its preferable

brain pharmacokinetics. In contrast, *in vitro* ARG of [^{125}I]BFC-OMe demonstrated some non-specific binding in brain sections of mBSE-mice as compared to that of the SC and BF derivatives.[20, 24, 27] Further studies to optimize BFC derivatives with high amyloid specificity and high contrast accumulation in the PrP^{Sc} against non-amyloid regions in the brain should identify promising prion-imaging agents for clinical use.

CONCLUSIONS

BFC derivatives were synthesized and evaluated as prion-imaging probes. All BFC derivatives exhibited high binding affinities to rMoPrP aggregates (K_d = 22.6–47.7 nM). Fluorescence imaging of BFC derivatives and the in vitro ARG of BFC-OMe showed clear images of PrP^{Sc} deposits in the mBSE-infected mouse brains. Since BFC derivatives have high binding affinities to PrP^{Sc} and a desirable brain distribution, it was suggested that BFC derivatives have promising properties as PrP^{Sc} imaging probes.

METHODS

General Methods and Instruments. All reagents were commercial products and were used without further purification, unless otherwise indicated. [^{125}I]NaI was purchased from Muromachi Yakuhin (Tokyo, Japan), MP Biomedicals (Costa Mesa, CA,

USA), and PerkinElmer Japan Co., Ltd. (Kanagawa, Japan). The ^{1}H NMR and ^{13}C NMR spectra were recorded on a JEOL JNM-AL 400 spectrometer (JEOL, Tokyo, Japan) with tetramethylsilane (TMS) as an internal standard. Mass spectra were obtained on JEOL IMS-DX or JMS-T100TD instruments (JEOL). High-performance liquid chromatography (HPLC) analysis and purification were performed using a Shimadzu HPLC system (LC-10AT pump with SPD-10A UV detector, $\lambda = 254$ nm) obtained from Shimadzu (Kyoto, Japan). An automated gamma counter with a NaI (Tl) detector (WIZARD^{2} 2470, PerkinElmer, Waltham, MA, USA) was used to measure the radioactivity. The experiments with animals were conducted in accordance with our institutional guidelines and were approved by Nagasaki University Animal Care Committee.

Chemistry. *2-Hydroxy-4-nitrobenzaldehyde (**1**).* BBr_3 (4.0 mL, 43.1 mmol) was added to 2-methoxy-4-nitrobenzaldehyde (500 mg, 2.76 mmol) in CH_2Cl_2 (4.0 mL) in an ice bath and stirred for 4 h at room temperature. After water was added to the mixture to stop the reaction, the mixture was extracted with $CHCl_3$ and washed with Sat. NaCl solution. The combined organic layers were dried with Na_2SO_4 and evaporated to dryness. The crude product was subjected to chromatographic purification on silica gel using $CHCl_3$/hexane (1/1) to give **1** (365 mg, 79%) as a yellow solid. ^{1}H NMR (400 MHz,

$CDCl_3$) δ 7.84-7.87 (m, 3H), 10.06 (s, 1H), 11.15 (s, 1H). MS (DART) *m/z*: 167 $[M + H]^+$.

*Ethyl 6-methoxybenzofuran-2-carboxylate (**2**).* A mixture of 2-hydroxy-4-methoxybenzaldehyde (200 mg, 1.31 mmol) and K_2CO_3 (362 mg, 2.62 mmol) in DMF (2.0 mL) was added to ethyl bromoacetate (435 μL, 3.93 mmol) and heated at 80 °C for 6 h. After 1,4-dioxane (8.0 mL) was added to azeotrope DMF, the reaction mixture was extracted with $CHCl_3$ and washed with Sat. NaCl solution. The combined organic layers were dried with Na_2SO_4 and evaporated to dryness. The crude product was subjected to chromatographic purification on silica gel using $CHCl_3$/hexane (1/1) to give **2** (43 mg, 15%) as a white solid. ^{1}H NMR (400 MHz, $CDCl_3$) δ 1.42 (t, *J* = 14.4 Hz, 3H), 3.86 (s, 3H), 4.42 (q, *J* = 21.6 Hz, 2H), 6.99 (dd, *J* = 2.8, 8.4 Hz, 1H), 7.06 (d, *J* = 2.0 Hz, 1H), 7.46 (s, 1H), 7.53 (d, *J* = 8.8 Hz, 1H). MS (DART) *m/z*: 221 $[M + H]^+$.

*Ethyl 6-nitrobenzofuran-2-carboxylate (**3**)*. A mixture of **1** (341 mg, 2.04 mmol) and K_2CO_3 (554 mg, 4.08 mmol) in DMF (3.0 mL) was added to ethyl bromoacetate (639 μL, 5.76 mmol) and heated at 90 °C for 18 h. After 1,4-dioxane (10 mL) was added to azeotrope DMF, the reaction mixture was extracted with $CHCl_3$ and washed with Sat. NaCl solution. The combined organic layers were dried with Na_2SO_4 and evaporated to dryness. The crude product was subjected to chromatographic purification on silica gel using $CHCl_3$/hexane (1/1) to give **3** (75 mg, 16%) as a pale yellow solid. ^{1}H NMR (400

MHz, $CDCl_3$) δ 1.46 (t, *J* = 14.0 Hz, 3H), 4.49 (q, *J* = 21.6 Hz, 2H), 7.60 (d, *J* = 0.8 Hz, 1H), 7.83 (d, *J* = 8.4 Hz, 1H), 8.24 (dd, *J* = 2.0, 8.8 Hz, 1H), 8.49 (s, 1H). MS (DART) *m/z*: 236 $[M + H]^+$.

*6-Methoxybenzofuran-2-carboxylic acid (**4**)*. Compound **2** (166 mg, 0.75 mmol) in MeOH (5.0 mL) was added to 1 M NaOH (4.0 mL) solution and stirred for 2 h at room temperature. After 1 M HCl solution (6.0 mL) was added to the reaction mixture in an ice bath, the mixture was extracted with $CHCl_3$ and washed with Sat. NaCl solution. The combined organic layers were dried with Na_2SO_4 and evaporated to dryness to give **4** (100 mg, 69%) as a pale yellow solid. ^1H NMR (400 MHz, $CDCl_3$) δ 3.89 (s, 3H), 6.97 (dd, *J* = 2.0, 8.8 Hz, 1H), 7.08 (s, 1H), 7.57 (d, *J* = 8.8 Hz, 1H), 7.63 (s, 1H). MS (DART) *m/z*: 193 $[M + H]^+$.

*6-Nitrobenzofuran-2-carboxylic acid (**5**).* Compound **3** (180 mg, 0.77 mmol) in MeOH (5.0 mL) was added to 1 M NaOH (5.0 mL) solution and stirred for 2 h at room temperature. After MeOH was evaporated to dryness and 1 M HCl solution (7.5 mL) was added to the reaction mixture in an ice bath, the mixture was extracted with $CHCl_3$ and washed with Sat. NaCl solution. The combined organic layers were dried with Na_2SO_4 and evaporated to dryness. The crude product was subjected to chromatographic purification on silica gel using EtOAc/hexane (7/3), 2% AcOH to give **5** (71 mg, 45%) as

a yellow solid. ^{1}H NMR (400 MHz, $CDCl_3$) δ 7.70 (s, 1H), 7.86 (d, *J* = 8.8 Hz, 1H), 8.26 (dd, *J* = 1.6, 8.6 Hz, 1H), 8.52 (s, 1H). MS (DART) *m/z*: 208 $[M + H]^+$.

*2-Acetyl-4-bromophenyl 6-methoxybenzofuran-2-carboxylate (**6**)*. Phosphoryl chloride (78 μL, 1.62 g/mL, 0.83 mmol) was added to pyridine (5.0 mL) in an ice bath. A mixture of **4** (53 mg, 0.28 mmol) and 1-(5-bromo-2hydroxy phenyl) ethenone (59 mg, 0.28 mmol) was added to phosphoryl chloride and stirred for 2 h at room temperature. After ice blocks were added to the reaction mixture, the precipitate was collected by filtration and washed with Sat. $NaHCO_3$ solution. The precipitate was dried to give **6** (76 mg, 71%) as a pale yellow solid. ^{1}H NMR (400 MHz, $CDCl_3$) δ 2.58 (s, 3H), 3.89 (s, 3H), 6.99 (dd, *J* = 2.4, 8.6 Hz, 1H), 7.09 (s, 1H), 7.20 (d, *J* = 8.4 Hz, 1H), 7.60 (d, *J* = 8.8 Hz, 1H), 7.70 (dd, *J* = 3.6, 8.8 Hz, 1H), 7.72 (s, 1H), 7.97 (d, *J* = 2.4 Hz, 1H).

2-Acetyl-4-bromophenyl 6-nitrobenzofuran-2-carboxylate (7). Phosphoryl chloride (77.8 μL, 1.62 g/mL, 0.83 mmol) was added to pyridine (5.0 mL) in an ice bath. A mixture of 5 (71 mg, 0.34 mmol) and 1-(5-bromo-2hydroxy phenyl) ethenone (73 mg, 0.34 mmol) was added to phosphoryl chloride and stirred for 12 h at room temperature. After ice blocks were added to the reaction mixture, the precipitate was collected by filtration and washed with Sat. $NaHCO_3$ solution. The precipitate was dried to give **7** (138 mg, 99%) as a pale yellow solid. ^{1}H NMR (400 MHz, $CDCl_3$) δ 2.59 (s, 3H), 7.21 (d, *J* = 8.8 Hz,

1H), 7.75 (dd, *J* = 2.4, 8.0 Hz, 1H), 7.83 (s, 1H), 7.90 (d, *J* = 8.8 Hz, 1H), 8.01 (d, *J* = 2.0 Hz, 1H), 8.29 (dd, *J* = 2.0, 8.8 Hz, 1H), 8.54 (s, 1H). MS (DART) *m/z*: 404, 406 $[M + H]^+$.

1-(5-Bromo-2-hydroxyphenyl)-3-(6-methoxybenzofuran-2-yl)propane-1,3-dione ***(8)***. Compound **6** (214 mg, 0.55 mmol) in pyridine (7.0 mL) was added to pulverized KOH (131 mg, 2.37 mmol) in an ice bath and stirred for 2 h at room temperature. In an ice bath, 10% AcOH solution was added to stop the reaction. The precipitate was filtered and dried. The crude product was subjected to chromatographic purification on silica gel using $CHCl_3$/hexane (1/1) to give **8** (36 mg, 17%) as a yellow solid. ^1H NMR (400 MHz, $CDCl_3$) δ 3.91 (s, 3H), 6.85 (s, 1H), 6.92 (d, *J* = 8.8 Hz, 1H), 6.96 (dd, *J* = 2.0, 8.8 Hz, 1H), 7.11 (d, *J* = 1.6 Hz, 1H), 7.50 (s, 1H), 7.54 (dd, *J* = 3.6, 8.2 Hz, 1H), 7.56 (d, *J* = 8.8 Hz, 1H), 7.93 (d, *J* = 2.4 Hz, 1H). MS (DART) *m/z*: 389, 391 $[M + H]^+$.

1-(5-Bromo-2-hydroxyphenyl)-3-(6-nitrobenzofuran-2-yl)propane-1,3-dione ***(9)***. Compound **7** (138 mg, 0.34 mmol) in pyridine (8.0 mL) was added to pulverized KOH (38 mg, 0.68 mmol) in an ice bath and stirred for 2 h at room temperature. In an ice bath, 10% AcOH solution was added to stop the reaction. The precipitate was filtered and dried. The crude product was subjected to chromatographic purification on silica gel using $CHCl_3$/hexane (3/1) to give **9** (56 mg, 41%) as a yellow solid. ^1H NMR (400 MHz, $CDCl_3$)

δ 7.21 (d, *J* = 8.8 Hz, 1H), 7.75 (dd, *J* = 2.4, 8.0 Hz, 1H), 7.83 (s, 1H), 7.90 (d, *J* = 8.8 Hz, 1H), 8.01 (d, *J* = 2.0 Hz, 1H), 8.29 (dd, *J* = 2.0, 8.8 Hz, 1H), 8.54 (s, 1H). MS (DART) *m/z*: 404, 406 $[M + H]^+$.

*6-Bromo-2-(6-methoxybenzofuran-2-yl)-4H-chromen-4-one (**10**)*. Compound **8** (29 mg, 74.5 μmol) suspended in AcOH (10 mL) was added to concentrated sulfuric acid (0.5 mL) and stirred under 100 °C for 2 h. After the mixture cooled to room temperature, ice blocks were added to the reaction mixture and the precipitate was filtered to give **10** (20 mg, 72%) as a yellow solid. ^{1}H NMR (400 MHz, $CDCl_3$) δ 3.93 (s, 3H), 6.87 (s, 1H), 6.95 (dd, *J* = 2.8, 8.4 Hz, 1H), 7.06 (d, *J* = 2.0 Hz, 1H), 7.41 (d, *J* = 8.8 Hz, 1H), 7.43 (s, 1H), 7.54 (d, *J* = 8.4 Hz, 1H), 7.77 (dd, *J* = 2.4, 8.8 Hz, 1H), 8.34 (d, *J* = 2.4 Hz, 1H). MS (DART) *m/z*: 371, 373 $[M + H]^+$.

6-Bromo-2-(6-nitrobenzofuran-2-yl)-4H-chromen-4-one (**11**). Compound **9** (580 mg, 1.44 mmol) suspended in AcOH (15 mL) was added to concentrated sulfuric acid (1 mL) and stirred under 100 °C for 2 h. After the mixture cooled to room temperature, ice blocks were added to the reaction mixture and the precipitate was filtered to give **11** (284 mg, 51%) as a pale yellow solid. ^{1}H NMR (400 MHz, $CDCl_3$) δ 7.05 (s, 1H), 7.21 (d, *J* = 8.0 Hz, 1H), 7.74 (dd, *J* = 2.4, 8.8 Hz, 1H), 7.84 (s, 1H), 7.91 (d, *J* = 2.0 Hz, 1H), 8.00 (d, *J* = 7.2 Hz, 1H), 8.27 (dd, *J* = 2.0, 8.0 Hz, 1H), 8.54 (d, *J* = 1.6 Hz, 1H). MS (DART) *m/z*:

386, 388 $[M + H]^+$.

2-(6-Methoxybenzofuran-2-yl)-6-(tributylstannyl)-4H-chromen-4-one ***(12)***. A mixture of **10** (46 mg, 0.12 mmol), $(Bu_3Sn)_2$ (1.16 g/mL) (417 μL, 0.83 mmol), and $(Ph_3P)_4Pd$ (58 mg, 50.2 μmol) in a solvent mixture (5.0 mL, 3:2 dioxane/Et_3N) was stirred under 90 °C for 14 h. After the mixture cooled to room temperature, the reaction mixture was filtered by celite, and the solution was evaporated to dryness. The crude product was subjected to chromatographic purification on silica gel using EtOAc/hexane (1/6) to give **12** (11 mg, 15%) as a pale yellow solid. ^{1}H NMR (400 MHz, $CDCl_3$) δ 0.89-1.61 (m, 27H), 3.90 (s, 3H), 6.90 (s, 1H), 6.95 (dd, *J* = 1.6, 8.6 Hz, 1H), 7.08 (d, *J* = 9.2 Hz, 1H), 7.43 (s, 1H), 7.48 (d, *J* = 8.4 Hz, 1H), 7.54 (d, *J* = 8.8 Hz, 1H), 7.77 (d, *J* = 8.4 Hz, 1H), 8.31 (s, 1H). MS (DART) *m/z*: 581 $[M + H]^+$.

6-Iodo-2-(6-methoxybenzofuran-2-yl)-4H-chromen-4-one (BFC-OMe). A solution of 0.2 M iodine in $CHCl_3$ (1.0 mL) was added to a solution of **12** (30 mg, 51.6 μmol) in $CHCl_3$ (4.0 mL) at room temperature, and the mixture was stirred at room temperature for 2 h. After Sat. $NaHSO_3$ (5.0 mL) solution added, the mixture was extracted with $CHCl_3$ and washed with sat. NaCl solution. The combined organic layers were dried with Na_2SO_4 and evaporated to dryness. The crude product was subjected to chromatographic purification on silica gel using EtOAc/hexane (1/3) to give BFC-OMe (19 mg, 88%) as a

pale yellow solid. ^{1}H NMR (400 MHz, $CDCl_3$) δ 3.90 (s, 3H), 6.88 (s, 1H), 6.95 (dd, *J* = 2.4, 8.6 Hz, 1H), 7.07 (d, *J* = 2.0 Hz, 1H), 7.43 (s, 1H), 7.41 (d, *J* = 2.0 Hz, 1H), 7.54 (d, *J* = 8.8 Hz, 1H), 8.22 (dd, *J* = 2.0, 8.0 Hz, 1H), 8.53 (d, *J* = 2.0 Hz, 1H). ^{13}C NMR (100 MHz, $CDCl_3$) δ 177.9, 160.3, 157.3, 155.4, 146.9, 142.4, 134.8, 133.9, 125.9, 122.5, 121.2, 120.0, 118.0, 114.0, 109.4, 106.6, 95.7, 55.9. HRMS (FAB) *m/z*: calcd for $C_{18}H_{12}IO_4$ $[M + H]^+$ 418.9780, found 418.9780.

*2-(6-Aminobenzofuran-2-yl)-6-bromo-4H-chromen-4-one (**13**).* A mixture of **11** (406 mg, 1.05 mmol), $SnCl_2$ (1.32 g, 5.25 mmol), and EtOH (10 mL) was stirred under 100 °C for 3 h. After the mixture cooled to room temperature and the solvent evaporated, 1 M NaOH and EtOAc was added to the reaction mixture and the suspension was filtered. The filtrate was extracted with EtOAc and washed with Sat. NaCl solution. The combined organic layers were dried with Na_2SO_4 and evaporated to dryness. The crude product was subjected to chromatographic purification on silica gel using EtOAc/hexane (1/3) to give **13** (334 mg, 89%) as a yellow solid. ^{1}H NMR (400 MHz, $CDCl_3$) δ 6.69 (dd, *J* = 1.2, 8.2 Hz, 1H), 6.84 (s, 1H), 6.87 (s, 1H), 7.40 (d, *J* = 14.8 Hz, 2H), 7.42 (d, *J* = 21.2 Hz, 1H), 7.76 (dd, *J* = 2.4, 9.4 Hz, 1H), 8.34 (d, *J* = 2.8 Hz, 1H). MS (DART) *m/z*: 356, 358 $[M + H]^+$.

*2-(6-Aminobenzofuran-2-yl)-6-(tributylstannyl)-4H-chromen-4-one (**14**).* The

procedure used for preparation of **12** was employed to give **14** (7.0 mg, 9%) as a yellow solid from **13** (50 mg, 0.14 mmol). ^{1}H NMR (400 MHz, $CDCl_3$) δ 0.87-1.613 (m, 27H), 6.66 (dd, *J* = 2.0, 10.0 Hz, 1H), 6.83 (s, 1H), 6.86 (s, 1H), 7.37 (s, 1H), 7.42 (d, *J* = 8.4 Hz, 1H), 7.46 (d, *J* = 8.4 Hz, 1H), 7.76 (dd, 0.8, 8.0 Hz, 1H), 8.30 (d, *J* = 1.2 Hz, 1H). MS (DART) *m/z*: 566 $[M + H]^+$.

2-(6-Aminobenzofuran-2-yl)-6-iodo-4H-chromen-4-one (BFC-NH_2). The procedure used for preparation of BFC-OMe was employed to give BFC-NH_2 (5.0 mg, 88%) as a yellow solid from **14** (8.0 mg, 14.1 μmol). ^{1}H NMR (400 MHz, $CDCl_3$) δ 3.99 (s, 2H), 6.69 (dd, *J* = 2.0, 8.0 Hz, 1H), 6.82 (s, 1H), 6.84 (s, 1H), 7.29 (s, 1H), 7.38 (s, 1H), 7.43 (d, *J* = 8.4 Hz, 1H), 7.94 (dd, *J* = 1.6, 8.4 Hz, 1H), 8.54 (d, *J* = 2.0 Hz, 1H). ^{13}C NMR (100 MHz, $CDCl_3$) δ 176.2, 173.8, 168.9, 157.9, 147.3, 143.3, 142.3, 134.8, 123.0, 120.0, 119.6, 113.7, 113.1, 110.3, 106.1, 96.8, 89.0. HRMS (FAB) *m/z*: calcd for $C_{17}H_{11}INO_3$ $[M + H]^+$ 403.9784, found 403.9782.

*6-Bromo-2-(6-(methylamino)benzofuran-2-yl)-4H-chromen-4-one (**15**).* To a mixture of **13** (40 mg, 0.11 mmol) and paraformaldehyde (18 mg, 0.60 mmol) in MeOH (20 mL) was added a solution of NaOMe in MeOH (30 μL, 27.0-29.7 w/w%, 0.22 mmol). The mixture was stirred under reflux for 1 h. After addition of $NaBH_4$ (25 mg, 0.66 mmol), the solution was stirred under reflux for 3 h. After the reaction mixture cooled to room

temperature, to the mixture was added 1 M NaOH solution. The mixture was extracted with $CHCl_3$ and washed with Sat. NaCl solution. The combined organic layers were dried with Na_2SO_4 and evaporated to dryness. The crude product was subjected to chromatographic purification on silica gel using EtOAc/$CHCl_3$ (1/9) to give **15** (9.0 mg, 22%) as a yellow solid. ^{1}H NMR (400 MHz, $CDCl_3$) δ 2.93 (s, 3H), 6.63 (dd, *J* = 2.0, 8.0 Hz, 1H), 6.69 (s, 1H), 6.83 (s, 1H), 7.38-7.42 (m, 3H), 7.76 (dd, *J* = 2.4, 8.8 Hz, 1H), 8.34 (d, *J* = 2.4 Hz, 1H). MS (DART) *m/z*: 370 $[M + H]^+$.

*2-(6-(Methylamino)benzofuran-2-yl)-6-(tributylstannyl)-4H-chromen-4-one (**16**).* The procedure used for preparation of **12** was employed to give **16** (9.0 mg, 41%) as a yellow solid from **15** (14 mg, 37.8 μmol). ^{1}H NMR (400 MHz, $CDCl_3$) δ 0.87-1.61 (m, 27H), 2.93 (s, 3H), 6.62 (dd, *J* = 2.0, 8.8 Hz, 1H), 6.71 (s, 1H), 6.85 (s, 1H), 7.38 (s, 1H), 7.41 (d, *J* = 8.4 Hz, 1H), 7.46 (d, *J* = 8.4 Hz, 1H), 7.75 (d, *J* = 7.6 Hz, 1H), 8.30 (s, 1H). MS (DART) *m/z*: 582 $[M + H]^+$.

6-Iodo-2-(6-(methylamino)benzofuran-2-yl)-4H-chromen-4-one (BFC-NHMe). The procedure used for preparation of BFC-OMe was employed to give BFC-NHMe (5.0 mg, 87%) as a yellow solid from **16** (8.0 mg, 13.8 μmol). ^{1}H NMR (400 MHz, $CDCl_3$) δ 2.92 (s, 3H), 6.63 (dd, *J* = 2.0, 8.2 Hz, 1H), 6.70 (s, 1H), 6.83 (s, 1H), 7.39-7.42 (m, 3H), 7.68 (d, *J* = 1.6 Hz, 1H), 8.22 (dd, *J* = 2.0, 8.2 Hz, 1H). ^{13}C NMR (100 MHz, $CDCl_3$) δ 177.9,

171.6, 158.5, 156.0, 155.8, 150.1, 145.5, 133.7, 125.9, 125.1, 124.4, 122.5, 117.9, 112.6, 110.1, 105.7, 92.8, 30.9. HRMS (FAB) *m/z*: calcd for $C_{18}H_{13}INO_3$ $[M + H]^+$ 417.9940, found 417.9941.

*6-Bromo-2-(6-(dimethylamino)benzofuran-2-yl)-4H-chromen-4-one (**17**).* To a mixture of **13** (65 mg, 0.18 mmol) and paraformaldehyde (54 mg, 1.80 mmol) in AcOH (12 mL) was added $NaCNBH_3$ (68 mg, 1.08 mmol) at room temperature. The mixture was stirred at room temperature for 4 h. To the reaction mixture was added 1 M NaOH. The mixture was extracted with $CHCl_3$ and washed with Sat. NaCl solution. The combined organic layers were dried with Na_2SO_4 and evaporated to dryness. The crude product was subjected to chromatographic purification on silica gel using EtOAc/hexane (1/3) to give **17** (50 mg, 71%) as a yellow solid. ^{1}H NMR (400 MHz, $CDCl_3$) δ 3.04 (s, 6H), 6.77-6.82 (m, 3H), 7.38 (s, 2H), 7.47 (d, *J* = 8.4 Hz, 1H), 7.74 (dd, *J* = 2.4, 9.2 Hz, 1H), 8.33 (d, *J* = 2.4 Hz, 1H). MS (DART) *m/z*: 384, 386 $[M + H]^+$.

*2-(6-(Dimethylamino)benzofuran-2-yl)-6-(tributylstannyl)-4H-chromen-4-one (**18**).* The procedure used for preparation of **12** was employed to give **18** (21 mg, 27%) as a yellow solid from **17** (50 mg, 0.13 mmol). ^{1}H NMR (400 MHz, $CDCl_3$) δ 0.87-1.61 (m, 27H), 3.06 (s, 6H), 6.78 (d, *J* = 2.4 Hz, 1H), 6.80 (s, 1H), 6.85 (s, 1H), 7.38 (s, 1H), 7.44-7.49 (m, 2H), 7.75 (dd, *J* = 1.6, 12.0 Hz, 1H), 8.30 (d, *J* = 1.6 Hz, 1H). MS (DART) *m/z*:

594 $[M + H]^+$.

2-(6-(Dimethylamino)benzofuran-2-yl)-6-iodo-4H-chromen-4-one (BFC-NMe$_2$). The procedure used for preparation of BFC-OMe was employed to give BFC-NMe_2 (8.0 mg, 92%) as a yellow solid from **18** (12 mg, 20.2 μmol). ^{1}H NMR (400 MHz, $CDCl_3$) δ 3.10 (s, 6H), 6.78 (s, 1H), 6.82 (s, 1H), 7.25 (s, 1H), 7.28 (s, 1H), 7.38 (s, 1H), 7.48 (d, J = 9.2 Hz, 1H), 7.92 (dd, J = 2.0, 8.6 Hz, 1H), 8.53 (d, J = 2.4 Hz, 1H). ^{13}C NMR (100 MHz, $CDCl_3$) δ 176.2, 158.6, 156.0, 155.5, 151.2, 142.2, 134.7, 126.1, 122.4, 120.0, 117.7, 116.6, 111.2, 110.5, 105.6, 93.9, 88.9, 40.9. HRMS (FAB) *m/z*: calcd for $C_{19}H_{15}INO_3$ $[M + H]^+$ 432.0097, found 432.0077.

Radiolabeling. The ^{125}I-labeled BFC derivatives were prepared according to the previous study.[21, 24] Briefly, to initiate the reaction, 50 μL H_2O_2 (3%) was added to a mixture of the tributyltin derivative (50 μg in 50 μL of EtOH), [^{125}I]NaI (3.7-7.4 MBq), and 1 M HCl (50 μL) in a sealed vial. The reaction was allowed to proceed at room temperature for 10-20 min and was terminated by addition of $NaHSO_3$. After neutralization with $NaHCO_3$, the solution was extracted with EtOAc. The extract was dried via passage through an anhydrous Na_2SO_4 column and it was then blown dry with a stream of nitrogen gas. The radioiodinated ligands were purified by HPLC on a Cosmosil 5C_{18}-AR-II column (4.6 × 150 mm) at a flow rate of 1.0 mL/min.

Binding assay using rMoPrP aggregates. Expression of the rMoPrP and aggregation of rMoPrP were carried out as described previously.[9, 38] The binding assays of BFC derivatives for rMoPrP aggregates were performed according to our previous studies.[20, 27] The saturation assays were performed by mixing an appropriate concentration of ^{125}I-labeled BFC derivatives (final concentration, 1.6−100 nM) and rMoPrP aggregates (100 nM) in NaCl/HEPES buffer (50 mM HEPES/KOH, 300 mM NaCl, pH 7.5) containing 20% (v/v) DMSO. After incubation for 2 h at room temperature, the mixture was then filtered through Whatman GF/B filters using a Brandel M-24 cell harvester and washed with NaCl/HEPES buffer (50 mM HEPES/KOH, 300 mM NaCl, pH 7.5) containing 20% (v/v) DMSO 4 times. Each assay tube before filtration and the filters containing the bound ^{125}I-BFC derivative was measured by an automatic gamma counter, and the bound/free ratio of ^{125}I-ligand was calculated. The dissociation constant (K_d) and binding capacity (B_{max}) of compounds were estimated by Scatchard analysis using PRISM4 (GraphPad Software Inc., San Diego, CA, USA).

Binding assay using Aβ$_{1-42}$ aggregates. Aggregation of Aβ$_{1-42}$ was carried out as described previously.[22, 39] The saturation assays were performed by mixing an appropriate concentration of [^{125}I]SC-NMe$_2$ or ^{125}I-labeled BFC derivatives (final concentration, 12.3−1000 nM) and Aβ$_{1-42}$ aggregates (100 nM) in 10% EtOH. After incubation for 2 h

at room temperature, the mixture was then filtered through Whatman GF/B filters using a Brandel M-24 cell harvester and washed with 10% EtOH 4 times. Each assay tube before filtration and the filters containing the bound ^{125}I-BFC derivative was measured by an automatic gamma counter, and the bound/free ratio of ^{125}I-ligand was calculated. K_d and B_{max}-of compounds were estimated by Scatchard analysis using PRISM4.

Animals. All animals were supplied by Kyudo Co., Ltd. (Saga, Japan). The mBSE infectious animal experiments were conducted under biosafety level 3 (BSL3) containment in accordance with the institutional guidelines. mBSE- and mock-infected mice were treated as previously reported.[26, 40] Experiments using animals were conducted in accordance with our institutional guidelines and were approved by the Nagasaki University Animal Care Committee.

Fluorescence staining and immunohistochemical analysis of mBSE- and mock-infected mouse brain sections. The mBSE-infected mice and the sections of their brains embedded in paraffin were prepared as reported previously.[20, 24, 27] The sections from mBSE- and mock-infected mice were dewaxed and incubated with a 50% EtOH solution (100 μM) of BFC derivatives for 1 h. Each section was washed with 50% EtOH for 2 min two times. The fluorescence images were obtained using an Eclipse 80i microscope (Nikon Corp., Tokyo, Japan) with a B-2A filter set (excitation, 450−490 nm; dichromic

mirror, 505 nm; longpass filter, 520 nm). Then, the deposits of PrP^{Sc} in the serial sections were detected by immunohistochemical staining using SAF32 anti-PrP antibody as described in our previous papers.[20]

Fluorescence staining analysis of *Tg2576* mouse brain sections. The *Tg2576* mice (female, 24-month-old) were used as the Alzheimer's model. After the mice were sacrificed by decapitation, the brains were immediately removed and frozen in powdered dry ice. The frozen blocks were sliced into serial sections, 10 μm thick. Each slide was incubated with a 50% EtOH solution (100 μM) of BFC derivatives for 1 h. The sections were washed in 50% EtOH for 2 min two times. The fluorescence images were collected by an Eclipse 80i microscope (Nikon Corp., Tokyo, Japan) with a B-2A filter set (excitation, 450−490 nm; dichromic mirror, 505 nm; longpass filter, 520 nm). Thereafter, the serial sections were also stained with thioflavin T, a pathological dye commonly used for staining Aβ plaques in the brain and examined using the microscope in the same condition with that of BFC derivatives.

In vitro ARG in mBSE-infected mouse brain sections. Each brain section after detected by immunohistochemical staining using SAF32 anti-PrP antibody was incubated in 50% (v/v) EtOH solution containing [^{125}I]BFC-OMe (11.9 kBq, 0.74 nM) for 1 h. The slices were rinsed for 2 min, two times each, with 50% (v/v) EtOH solution. The sections

were dried under a steam of cold air and placed in contact with imaging plates (BAS-MS 2040; GE Health Care) for 51 h. The distribution of radioactivity on the plates was analyzed using the Fluoro Image Analyzer (FLA5100; GE Health Care).

In vitro ARG in *Tg2576* mouse brain sections. Brain sections (10 μm thick) from *Tg2576* mice (female, 24 months old) or age-matched wild-type mice (female, 24 months old) were incubated with [^{125}I]BFC-OMe (11.9 kBq, 0.74 nM), washed, and placed on imaging plates. Radioactivity was detected as described in the ARG study of mBSE-infected mice. Subsequently, serial sections were stained with thioflavin T (10 μM), a pathological dye commonly used for staining Aβ plaques in the brain, and examined using a fluorescence microscope.

In vivo biodistribution in mice. A saline solution (100 μL) of ^{125}I-labeled BFC derivatives (6.2−22.8 kBq) containing DMSO (20 μL) was injected directly into the tail vein of ddY mice (male, 5 weeks old, 20−25 g). The mice were sacrificed at 2, 30, 60, 120, and 180 min post injection. The organs of interest were removed and weighed, and the radioactivity was measured using a gamma counter (PerkinElmer, WIZARD^2 2470).

CNS PET MPO score calculation. ClogP and TPSA were calculated using a ChemBioDraw Ultra 20.1. ClogD and pK_a were calculated using a SPARK on line calculator. The CNS MPO score calculation has been carried out according to the

literature.[31]

ASSOCIATED CONTENT

Supporting Information: Detailed biodistribution data in mice and in vitro autoradiography in Tg2576 mice (PDF).

Notes

The authors declare no competing financial interest.

ACKNOWLEDGMENTS

Financial supports were provided by the Grant-in-Aid for Scientific Research (B) (Grant No. 21390348) and Grant-in-Aid for Exploratory Research (Grant No. 20659192, 21K19452) from the Japan Society for the Promotion of Science (JSPS), GSK Japan Research Grant 2015 and a grant from Takeda Science Foundation.

REFERENCES

(1) Tee, B. L.; Longoria Ibarrola, E. M.; Geschwind, M. D. Prion Diseases. *Neurol. Clin.* **2018**, *36* (4), 865-897. DOI: 10.1016/j.ncl.2018.07.005.

(2) Jankovska, N.; Rusina, R.; Bruzova, M.; Parobkova, E.; Olejar, T.; Matej, R. Human Prion Disorders: Review of the Current Literature and a Twenty-Year Experience of the National Surveillance Center in the Czech Republic. *Diagnostics* **2021**, *11* (10). DOI: 10.3390/diagnostics11101821.

(3) Uttley, L.; Carroll, C.; Wong, R.; Hilton, D. A.; Stevenson, M. Creutzfeldt-Jakob disease: a systematic review of global incidence, prevalence, infectivity, and incubation. *The Lancet Infect. Dis.* **2020**, *20* (1), e2-e10. DOI: 10.1016/s1473-3099(19)30615-2.

(4) Nozaki, I.; Hamaguchi, T.; Sanjo, N.; Noguchi-Shinohara, M.; Sakai, K.; Nakamura, Y.; Sato, T.; Kitamoto, T.; Mizusawa, H.; Moriwaka, F.; Shiga, Y.; Kuroiwa, Y.; Nishizawa, M.; Kuzuhara, S.; Inuzuka, T.; Takeda, M.; Kuroda, S.; Abe, K.; Murai, H.; Murayama, S.; Tateishi, J.; Takumi, I.; Shirabe, S.; Harada, M.; Sadakane, A.; Yamada, M. Prospective 10-year surveillance of human prion diseases in Japan. *Brain* **2010**, *133* (10), 3043-3057. DOI: 10.1093/brain/awq216.

(5) Collinge, J. Prion diseases of humans and animals: their causes and molecular basis. *Annu. Rev. Neurosci.* **2001**, *24*, 519-550. DOI: 10.1146/annurev.neuro.24.1.519.

(6) Kraus, A.; Groveman, B. R.; Caughey, B. Prions and the potential transmissibility of protein misfolding diseases. *Annu. Rev. Microbiol.* **2013**, *67*, 543-564. DOI: 10.1146/annurev-micro-092412-155735.

(7) Colby, D. W.; Prusiner, S. B. Prions. *Cold Spring Harb. Perspect. Biol.* **2011**, *3* (1), 1-22, Article. DOI: 10.1101/cshperspect.a006833.

(8) Puoti, G.; Bizzi, A.; Forloni, G.; Safar, J. G.; Tagliavini, F.; Gambetti, P. Sporadic human prion diseases: molecular insights and diagnosis. *Lancet. Neurol.* **2012**, *11* (7), 618-628. DOI: 10.1016/s1474-4422(12)70063-7.

(9) Atarashi, R.; Satoh, K.; Sano, K.; Fuse, T.; Yamaguchi, N.; Ishibashi, D.; Matsubara, T.; Nakagaki, T.; Yamanaka, H.; Shirabe, S.; Yamada, M; Mizusawa, H.; Kitamoto, T.; Klug, G.; McGlade, A.; Collins, S. J.; Nishida, N. Ultrasensitive human prion detection in cerebrospinal fluid by real-time quaking-induced conversion. *Nat. Med.* **2011**, *17* (2), 175-178. DOI: 10.1038/nm.2294.

(10) Dong, T. T.; Satoh, K. The Latest Research on RT-QuIC Assays-A Literature Review. *Pathogens* **2021**, *10* (3), 305. DOI: 10.3390/pathogens10030305. Satoh, K.; Atarashi, R.; Nishida, N. Real-Time Quaking-Induced Conversion for Diagnosis of Prion Disease. *Methods Mol. Biol.* **2017**, *1658*, 305-310. DOI: 10.1007/978-1-4939-7244-9_21.

(11) Hermann, P.; Appleby, B.; Brandel, J. P.; Caughey, B.; Collins, S.; Geschwind, M. D.; Green, A.; Haïk, S.; Kovacs, G. G.; Ladogana, A.; Llorens, F.; Mead, S.; Nishida, N.; Pal, S.; Parchi, P.; Pocchiari, M.; Satoh, K.; Zanusso, G.; Zerr, I. Biomarkers and diagnostic guidelines for sporadic Creutzfeldt-Jakob

disease. *Lancet Neurol.* **2021**, *20* (3), 235-246. DOI: 10.1016/S1474-4422(20)30477-4.

(12) Grau-Rivera, O.; Calvo, A.; Bargalló, N.; Monté, G. C.; Nos, C.; Lladó, A.; Molinuevo, J. L.; Gelpi, E.; Sánchez-Valle, R. Quantitative Magnetic Resonance Abnormalities in Creutzfeldt-Jakob Disease and Fatal Insomnia. *J. Alzheimers Dis.* **2017**, *55* (1), 431-443. DOI: 10.3233/jad-160750. Sacco, S.; Paoletti, M.; Staffaroni, A. M.; Kang, H.; Rojas, J.; Marx, G.; Goh, S. Y.; Luisa Mandelli, M.; Allen, I. E.; Kramer, J. H.; Bastianello, S.; Henry, R. G.; Rosen, H. J.; Caverzasi, E.; Geschwind, M. D. Multimodal MRI staging for tracking progression and clinical-imaging correlation in sporadic Creutzfeldt-Jakob disease. *NeuroImage Clin.* **2021**, *30*, 102523. DOI: 10.1016/j.nicl.2020.102523.

(13) Fuchigami, T. Development of Molecular Probes for Live Imaging of Cancer and Infectious Diseases. *Yakugaku Zasshi* **2019**, *139* (12), 1531-1538. DOI: 10.1248/yakushi.19-00158. Park, S.-M.; Aalipour, A.; Vermesh, O.; Yu, J. H.; Gambhir, S. S. Towards clinically translatable in vivo nanodiagnostics. *Nat. Rev. Mater.* **2017**, *2* (5), 17014. DOI: 10.1038/natrevmats.2017.14.

(14) Prusiner, S. B. Prions. *Proc. Natl. Acad. Sci. U. S. A.* **1998**, *95* (23), 13363-13383. DOI: 10.1073/pnas.95.23.13363.

(15) Letourneau-Guillon, L.; Wada, R.; Kucharczyk, W. Imaging of prion diseases. *J.*

Magn. Reson. Imaging **2012**, *35* (5), 998-1012. DOI: 10.1002/jmri.23504.

(16) Kepe, V.; Ghetti, B.; Farlow, M. R.; Bresjanac, M.; Miller, K.; Huang, S. C.; Wong, K. P.; Murrell, J. R.; Piccardo, P.; Epperson, F.; Repovs, G.; Smid, L. M.; Petric, A.; Siddarth, P.; Liu, J.; Satyamurthy, N.; Small, G. W.; Barrio, J. R. PET of brain prion protein amyloid in Gerstmann-Sträussler-Scheinker disease. *Brain Pathol.* **2010**, *20* (2), 419-430. DOI: 10.1111/j.1750-3639.2009.00306.x.

(17) D Deters, K. D.; Risacher, S. L.; Yoder, K. K.; Oblak, A. L.; Unverzagt, F. W.; Murrell, J. R.; Epperson, F.; Tallman, E. F.; Quaid, K. A.; Farlow, M. R.; Saykin, A. J.; Ghetti, B. [^{11}C]PiB PET in Gerstmann-Straussler-Scheinker disease. *Am. J. Nucl. Med. Mol. Imaging* **2016**, *6* (1), 84-93. Okamura, N.; Shiga, Y.; Furumoto, S.; Tashiro, M.; Tsuboi, Y.; Furukawa, K.; Yanai, K.; Iwata, R.; Arai, H.; Kudo, Y.; Itoyama, Y.; Doh-ura, K. In vivo detection of prion amyloid plaques using [^{11}C]BF-227 PET. *Eur. J. Nucl. Med. Mol. Imaging* **2010**, *37* (5), 934-941. DOI: 10.1007/s00259-009-1314-7.

(18) Fuchigami, T.; Ogawa, A.; Yamashita, Y.; Haratake, M.; Watanabe, H.; Ono, M.; Kawasaki, M.; Yoshida, S.; Nakayama, M. Development of alkoxy styrylchromone derivatives for imaging of cerebral amyloid-β plaques with SPECT. *Bioorg. Med. Chem. Lett.* **2015**, *25* (16), 3363-3367. DOI: 10.1016/j.bmcl.2015.05.048.

(19) Fuchigami, T.; Yamashita, Y.; Haratake, M.; Ono, M.; Yoshida, S.; Nakayama, M.

Synthesis and evaluation of ethyleneoxylated and allyloxylated chalcone derivatives for imaging of amyloid β plaques by SPECT. *Bioorg. Med. Chem.* **2014**, *22* (9), 2622-2628, Article. DOI: 10.1016/j.bmc.2014.03.032. Ono, M.; Ikeoka, R.; Watanabe, H.; Kimura, H.; Fuchigami, T.; Haratake, M.; Saji, H.; Nakayama, M. Synthesis and evaluation of novel chalcone derivatives with ^{99m}Tc/Re complexes as potential probes for detection of β-amyloid plaques. *ACS Chem. Neurosci.* **2010**, *1* (9), 598-607. DOI: 10.1021/cn100042d.

(20) Fuchigami, T.; Yamashita, Y.; Kawasaki, M.; Ogawa, A.; Haratake, M.; Atarashi, R.; Sano, K.; Nakagaki, T.; Ubagai, K.; Ono, M.; Yoshida, S.; Nishida, N.; Nakayama M. Characterisation of radioiodinated flavonoid derivatives for SPECT imaging of cerebral prion deposits. *Sci. Rep.* **2015**, *5*, Article. DOI: 10.1038/srep18440.

(21) Nakaie, M.; Katayama, F.; Nakagaki, T.; Kawasaki, M.; Yoshida, S.; Toriba, A.; Ogawa, K.; Nishida, N.; Nakayama, M.; Fuchigami, T. Synthesis and Characterization of Hydroxyethylamino- and Pyridyl-Substituted 2-Vinyl Chromone Derivatives for Detection of Cerebral Abnormal Prion Protein Deposits. *Chem. Pharm. Bull.* **2022**, *70* (3), 211-219. DOI: 10.1248/cpb.c21-00902.

(22) Fuchigami, T.; Kobashi, N.; Haratake, M.; Kawasaki, M.; Nakayama, M. Synthesis and biological evaluation of radioiodinated quinacrine-based derivatives for SPECT imaging of Aβ plaques. *Eur. J. Med. Chem.* **2013**, *60*, 469-478. DOI:

10.1016/j.ejmech.2012.12.020.

(23) Kawasaki, M.; Fuchigami, T.; Kobashi, N.; Nakagaki, T.; Sano, K.; Atarashi, R.; Yoshida, S.; Haratake, M.; Nishida, N.; Nakayama, M. Development of radioiodinated acridine derivatives for in vivo imaging of prion deposits in the brain. *Bioorg. Med. Chem.* **2017**, *25* (3), 1085-1093, Article. DOI: 10.1016/j.bmc.2016.12.020.

(24) Fuchigami, T.; Kawasaki, M.; Koyama, R.; Nakaie, M.; Nakagaki, T.; Sano, K.; Atarashi, R.; Yoshida, S.; Haratake, M.; Ono, M.; Nishida, N.; Nakayama, M. Development of Radioiodinated Benzofuran Derivatives for in Vivo Imaging of Prion Deposits in the Brain. *ACS Infect. Dis.* **2019**. DOI: 10.1021/acsinfecdis.8b00184.

(25) Ono, M.; Fuchi, Y.; Fuchigami, T.; Kobashi, N.; Kimura, H.; Haratake, M.; Saji, H.; Nakayama, M. Novel Benzofurans with ^{99m}Tc Complexes as Probes for Imaging Cerebral β-Amyloid Plaques. *ACS Med. Chem. Lett.* **2010**, *1* (8), 443-447. DOI: 10.1021/ml100140d.

(26) Fujihara, A.; Atarashi, R.; Fuse, T.; Ubagai, K.; Nakagaki, T.; Yamaguchi, N.; Ishibashi, D.; Katamine, S.; Nishida, N. Hyperefficient PrP Sc amplification of mouse-adapted BSE and scrapie strain by protein misfolding cyclic amplification technique. *FEBS J.* **2009**, *276* (10), 2841-2848. DOI: 10.1111/j.1742-4658.2009.07007.x.

(27) Fuchigami, T.; Kawasaki, M.; Watanabe, H.; Nakagaki, T.; Nishi, K.; Sano, K.;

Atarashi, R.; Nakaie, M.; Yoshida, S.; Ono, M.; Nishida, N.; Nakayama, M. Feasibility studies of radioiodinated pyridyl benzofuran derivatives as potential SPECT imaging agents for prion deposits in the brain. *Nucl. Med. Biol.* **2020**, *90-91*, 41-48. DOI: 10.1016/j.nucmedbio.2020.09.003.

(28) Ono, M.; Cheng, Y.; Kimura, H.; Watanabe, H.; Matsumura, K.; Yoshimura, M.; Iikuni, S.; Okamoto, Y.; Ihara, M.; Takahashi, R.; Saji, H. Development of novel ^{123}I-labeled pyridyl benzofuran derivatives for SPECT imaging of β-amyloid plaques in Alzheimer's disease. *PLoS One* **2013**, *8* (9), e74104. DOI: 10.1371/journal.pone.0074104.

(29) Ono, M. Development of positron-emission tomography/single-photon emission computed tomography imaging probes for in vivo detection of beta-amyloid plaques in Alzheimer's brains. *Chem. Pharm. Bull.* **2009**, *57* (10), 1029-1039. DOI: 10.1248/cpb.57.1029.

(30) Wager, T. T.; Hou, X.; Verhoest, P. R.; Villalobos, A. Moving beyond rules: the development of a central nervous system multiparameter optimization (CNS MPO) approach to enable alignment of druglike properties. *ACS Chem. Neurosci.* **2010**, *1* (6), 435-449. DOI: 10.1021/cn100008c.

(31) Zhang, L.; Villalobos, A.; Beck, E. M.; Bocan, T.; Chappie, T. A.; Chen, L.; Grimwood, S.; Heck, S. D.; Helal, C. J.; Hou, X.; Humphrey, J. M.; Lu, J.;

Skaddan, M. B.; McCarthy, T. J.; Verhoest, P. R.; Wager, T. T.; Zasadny, K. Design and selection parameters to accelerate the discovery of novel central nervous system positron emission tomography (PET) ligands and their application in the development of a novel phosphodiesterase 2A PET ligand. *J. Med. Chem.* **2013**, *56* (11), 4568-4579. DOI: 10.1021/jm400312y.

(32) Hsiao, K.; Chapman, P.; Nilsen, S.; Eckman, C.; Harigaya, Y.; Younkin, S.; Yang, F.; Cole, G. Correlative memory deficits, Abeta elevation, and amyloid plaques in transgenic mice. *Science* **1996**, *274* (5284), 99-102. DOI: 10.1126/science.274.5284.99.

(33) Porcellotti, S.; Fanelli, F.; Fracassi, A.; Sepe, S.; Cecconi, F.; Bernardi, C.; Cimini, A.; Cerù, M. P.; Moreno, S. Oxidative Stress during the Progression of β-Amyloid Pathology in the Neocortex of the Tg2576 Mouse Model of Alzheimer's Disease. *Oxid. Med. Cell. Longev.* **2015**, *2015*, 967203. DOI: 10.1155/2015/967203.

(34) Zhang, W.; Oya, S.; Kung, M. P.; Hou, C.; Maier, D. L.; Kung, H. F. F-18 Polyethyleneglycol stilbenes as PET imaging agents targeting Abeta aggregates in the brain. *Nucl. Med. Biol.* **2005**, *32* (8), 799-809. DOI: 10.1016/j.nucmedbio.2005.06.001.

(35) Ono, M.; Cheng, Y.; Kimura, H.; Cui, M.; Kagawa, S.; Nishii, R.; Saji, H. Novel 18F-labeled benzofuran derivatives with improved properties for positron emission tomography (PET) imaging of β-amyloid plaques in Alzheimer's brains. *J. Med. Chem.*

2011, *54* (8), 2971-2979. DOI: 10.1021/jm200057u.

(36) Yoshimura, M.; Ono, M.; Matsumura, K.; Watanabe, H.; Kimura, H.; Cui, M.; Nakamoto, Y.; Togashi, K.; Okamoto, Y.; Ihara, M.; Takahashi, R.; Saji, H. Structure-Activity Relationships and in Vivo Evaluation of Quinoxaline Derivatives for PET Imaging of β-Amyloid Plaques. *ACS Med. Chem. Lett.* **2013**, *4* (7), 596-600. DOI: 10.1021/ml4000707.

(37) Garg, P. K.; Harrison, C. L.; Zalutsky, M. R. Comparative tissue distribution in mice of the alpha-emitter ^{211}At and ^{131}I as labels of a monoclonal antibody and F(ab')2 fragment. *Cancer Res* **1990**, *50* (12), 3514-3520.

(38) Sano, K.; Atarashi, R.; Ishibashi, D.; Nakagaki, T.; Satoh, K.; Nishida, N. Conformational properties of prion strains can be transmitted to recombinant prion protein fibrils in real-time quaking-induced conversion. *J. Virol.* **2014**, *88* (20), 11791-11801. DOI: 10.1128/jvi.00585-14. Atarashi, R.; Moore, R. A.; Sim, V. L.; Hughson, A. G.; Dorward, D. W.; Onwubiko, H. A.; Priola, S. A.; Caughey, B. Ultrasensitive detection of scrapie prion protein using seeded conversion of recombinant prion protein. *Nat. Methods* **2007**, *4* (8), 645-650. DOI: 10.1038/nmeth1066.

(39) Ono, M.; Maya, Y.; Haratake, M.; Nakayama, M. Synthesis and characterization of styrylchromone derivatives as beta-amyloid imaging agents. *Bioorg. Med. Chem.* **2007**,

15 (1), 444-450. DOI: 10.1016/j.bmc.2006.09.044.

(40) Nakagaki, T.; Satoh, K.; Ishibashi, D.; Fuse, T.; Sano, K.; Kamatari, Y. O.; Kuwata, K.; Shigematsu, K.; Iwamaru, Y.; Takenouchi, T.; Kitani, H.; Nishida, N. FK506 reduces abnormal prion protein through the activation of autolysosomal degradation and prolongs survival in prion-infected mice. *Autophagy* **2013**, *9* (9), 1386-1394. DOI: 10.4161/auto.25381.

Table of Contents